

Sensitivity to anomalous Higgs couplings via $WW \rightarrow HH$ at e^+e^- colliders

Manuel González López

Máster en Física Teórica



MÁSTERES
DE LA UAM
2018 - 2019

Facultad de Ciencias

Sensitivity to anomalous Higgs couplings via $WW \rightarrow HH$ at e^+e^- colliders

Manuel González López

Trabajo de Fin de Máster
Máster en Física Teórica IFT-UAM

Trabajo dirigido por la Dra. **María José Herrero Solans**
Catedrática del Departamento de Física Teórica



13 de septiembre de 2019

Abstract

The goal of this work is to test the sensitivity of certain scattering processes to Beyond the Standard Model interactions among Higgs and electroweak gauge bosons. We will do so by employing the Electroweak Chiral Lagrangian (EChL), an effective field theory based on Chiral Perturbation Theory, which allows to introduce parameters that quantify possible deviations from the Standard Model (SM) in a model independent way. First, we present this theoretical framework, and describe how it allows to compute observables that may be sensitive to New Physics. Then, we focus on a particular process, $WW \rightarrow HH$, and compare its behaviour within the SM and the EChL. We will first describe the dynamics of the subprocess, and then embed it in a process that could take place in an e^+e^- collider, analyzing how the cross section depends on the EChL parameters by making a scan on the parameter space. Finally, we conclude by estimating the number of events that could be detected in this kind of accelerator once the Higgs bosons decay, trying to be predictive on the experimental consequences of the possible anomalous couplings.

Contents

1	Introduction	1
2	The Electroweak Chiral Lagrangian	4
2.1	The Chiral Lagrangian in QCD	5
2.2	Building the Electroweak Chiral Lagrangian	6
2.3	Computing observables using the EChL	9
2.4	Linear vs. non-linear representations	12
3	Vector Boson Scattering: $W^+W^- \rightarrow HH$ subprocess	13
3.1	SM predictions	15
3.2	EChL predictions	16
4	Vector Boson Scattering at an e^+e^- accelerator	20
4.1	The Effective W approximation compared to MC simulations	22
4.2	Sensitivity to the EChL parameters	27
5	Conclusions	36
A	Diagrams contributing to the $e^+e^- \rightarrow HH\nu_e\bar{\nu}_e$ process	42
B	Computations with the effective W approximation	48

1 Introduction

Currently, our understanding of the fundamental constituents of Nature is based on the so called Standard Model of Particle Physics (SM) [1–3]. This theory, developed along the 20th century thanks to both theoretical and experimental efforts, describes with great success the fundamental particles (those which are not composite states) and the interactions among them.

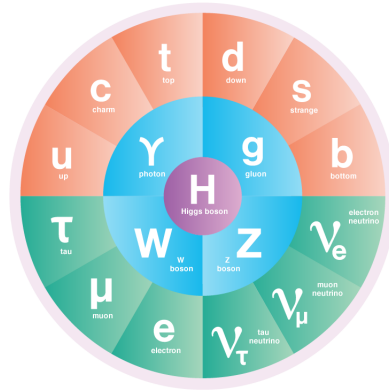


Figure 1.1: Particle content of the Standard Model.

The Standard Model is a quantum field theory based on the symmetry group $SU(3)_C \times SU(2)_L \times U(1)_Y$. These symmetries are gauge (local) and determine the characteristics of the fundamental particles and how they interact with each other. The $SU(3)_C$ subgroup describes the strong interactions between quarks and gluons, while the $SU(2)_L \times U(1)_Y$ is responsible for the electroweak interactions. The study of the latter will be the motivation for this work.

Electroweak interactions affect all particles which exhibit weak isospin (the charge associated to the $SU(2)_L$ subgroup) and/or hypercharge (the quantum number related to $U(1)_Y$). All fermions are hypercharged, while only the left-handed ones show weak isospin. According to the gauge principle, there are three mediator bosons related to the $SU(2)_L$ group (W^1, W^2, W^3) and one, B , associated to $U(1)_Y$. Gauge symmetry forces all these particles to be massless (any mass term for them would explicitly break gauge invariance).

However, electroweak symmetry is not preserved in Nature: it is spontaneously broken. This means that, although the Lagrangian which describes this interaction is exactly invariant under gauge transformations, its ground state is not. This breaking takes place via the Higgs mechanism [4–9]. A scalar complex doublet, which contains four degrees of freedom, is introduced in the theory, coupled to the electroweak gauge bosons. This scalar has an associated potential, which has infinite degenerate non-zero minima. This means that the neutral component of the doublet will take a vacuum expectation value (vev) which, through the couplings between the doublet and the electroweak bosons, will render the latter massive. More specifically, the spontaneous symmetry breaking (SSB) will generate, according to the Goldstone

Theorem [10], as many (massless) Nambu-Goldstone bosons as generators of the broken group. These modes will then mix with the massless gauge bosons, which will acquire a third (longitudinal) degree of freedom, becoming massive. In simpler words, the gauge bosons “eat” the Goldstone modes and acquire a mass. The Higgs boson is the fourth degree of freedom of the scalar doublet. It is included in the spectrum as a remnant of the electroweak symmetry breaking, appearing as a massive particle. The breaking of the electroweak symmetry is not complete: only three of the four bosons (the usual W^+ , W^- and Z) obtain a mass, while the fourth one (the photon) stays massless. This means that, even after SSB, the theory is still invariant under a $U(1)$ gauge group, associated to electromagnetic interactions (those mediated by the photon). The physical, massive bosons cannot be associated one-to-one with the massless ones that exist before the SSB: each set of particles can be expressed as a linear combination of the other. The misalignment between the “interaction basis” (the W^1, W^2, W^3 and B bosons) and the “mass basis” (the physical W, Z and γ) can be understood by a rotation parametrized by the weak angle θ_W . This angle (which is a free parameter of the theory and can only be determined experimentally) relates the masses of the W and Z bosons, as well as the coupling constants of the broken $SU(2)_L \times U(1)_Y$ and the unbroken $U(1)_{em}$.

The Higgs mechanism was theoretically developed in the 60s, and the W and Z bosons were discovered in 1983 [11–14], with masses of around 80 and 90 GeV respectively. By that time, the phenomenon of the SSB was well understood, although it took 30 years to discover the Higgs boson. In July 2012, the experimental collaborations of ATLAS and CMS announced the discovery of a scalar, neutral particle, with a mass of around 125 GeV [15, 16], perfectly compatible with the characteristics of the Higgs boson responsible for the Higgs mechanism and the electroweak symmetry breaking sector (EWSBS). This completed the experimental and theoretical understanding of the Standard Model of Particle Physics.

Nevertheless, there are both experimental evidences and theoretical issues that unequivocally point out that the Standard Model cannot be the fundamental theory of elementary particles. Among the experimental evidences are the non-zero masses of neutrinos or the presence of dark matter. Most of the theoretical problems are related to the fine-tuning of some of the free parameters of the theory, for instance, the flavour puzzle or the strong CP problem.

One of these issues has to do with the Higgs boson: the hierarchy problem. The mass of the Higgs boson is not established by first principles, being a free parameter of the theory. It was fixed experimentally at around 125 GeV when this particle was discovered. However, this value is surprisingly small; the Higgs mass is not protected by any symmetry (in other words, no symmetry would be restored if the Higgs were massless), so it is very sensitive to quantum ultraviolet (UV) corrections. Reproducing the experimental value of the Higgs mass would require a huge fine-tuning in its bare mass. This fact might be a hint towards a theory Beyond the Standard Model (BSM), some UV dynamics that could explain in a natural way the value of the Higgs mass. Some of these theories include new symmetries which are spontaneously broken, with the Higgs boson being the associated (pseudo) Nambu-

Goldstone boson. This new symmetry would protect its mass, solving the hierarchy problem. Other lines of investigation dislike the fact that only one fundamental scalar exists in the Standard Model, and explore the possibility of the Higgs boson being a composite state. However, up to date, none of these attempts has been proved successful, and the hierarchy problem remains open.

Due to this lack of a reliable UV theory, effective theories (see, for instance, [17] or [18]) have turned out to be a powerful tool in the study of the nature of the Higgs boson and the EWSBS. Effective theories assume the existence of UV new Physics above a certain scale, but do not describe the dynamics above that threshold. Thus, they do not include new particle content, as new states would only be able to propagate at energies of, approximately, their mass. However, effective theories take into account the low-energy effect of the possible existence of new particles, including new interaction vertices or modifications of those which already existed. The paradigmatic example of an effective theory is Fermi's theory of weak interactions [19]. Before the W boson was discovered, Fermi described beta decays via a four-fermion point interaction, whose intensity was quantified by the coupling G_F . What this theory really describes is a process mediated by a W boson, but when the energy of the process is much lower than the mass of this particle, its propagator can be collapsed into a point, yielding a four-fermion interaction. The effect of the W boson is encoded in the coupling G_F . In fact, $G_F = \frac{\sqrt{2}g^2}{8M_W^2}$.

When studying the spontaneous breaking sector of a certain symmetry, chiral Lagrangians are a particularly useful tool. First developed in the late 70s [20], these are effective theories that describe the low-energy dynamics of Goldstone bosons of a particular SSB. Their effective character lies in the fact that all possible heavier particles are integrated out, and only the lighter particles are involved. They rely on the formalism of Chiral Perturbation Theory, working out expansions in the momenta of the involved particles (assuming these live way below the UV scale). These Lagrangians are equipped to include deviations from the SM in the form of certain parameters, which would reflect the effects of new physics above the UV scale.

One of the main advantages of Chiral Lagrangians is their model-independence: they provide information that can be interpreted in different manners by different UV theories. In fact, some models predict certain relations between the parameters that can be introduced in the Lagrangian. This way, this effective theory is a perfect approach in order to make contact with experimental data, as it allows to make predictions for observables in terms of these parameters. Comparisons with experiment may set constraints on them, which may eventually exclude or favor certain UV theories.

Chiral Lagrangians were first employed in QCD [20], where chiral symmetry is spontaneously broken. This SSB yields the existence of three pions, which are, strictly speaking, pseudo-Nambu-Goldstone bosons (due to the fact that the symmetry is also explicitly broken by quark masses). The QCD Chiral Lagrangian describes the dynamics of pions well below the typical mass scale of the rest of the

hadrons (around 1 GeV), which have been integrated out. In a similar manner, the Electroweak Chiral Lagrangian (EChL) (which was developed in the 80s [21–23]) provides an effective description of the Nambu-Goldstone bosons which arise from the electroweak SSB. After the Higgs mechanism takes place, these will mix with the electroweak gauge bosons, yielding the physical vector bosons W and Z . Thus, the EChL is useful to describe their dynamics, and, as they couple to the Higgs boson, it is a powerful tool to probe the EWSBS. Nonetheless, there are still open issues in the employment of the EChL. As the UV theory is unknown, there is no way to match the observables computed in the effective theory. This means that these parameters are free, and need to be constrained experimentally and theoretically (for instance, imposing unitarity). Besides, the UV scale is also unknown, so it is unclear up to what energy the effective theory can be reliable.

Regarding the EChL phenomenology, Vector Boson Scattering (VBS) is particularly useful in order to study the EWSBS sector. These are processes with two vector bosons in the initial state resulting in two vector and/or Higgs bosons. Their interest relies in the fact that the vertices in these processes directly involve the operators of the EChL, being sensitive to possible deviations from the SM. In this work we will focus on the $W^+W^- \rightarrow HH$ process. Although it also exhibits interesting features, we will not consider the $ZZ \rightarrow HH$ case.

This work will be organized as follows. In section 2 we will present the EChL, showing how the fields are introduced and how deviations from the SM can be parametrized. In section 3 we will fully analyze the $W^+W^- \rightarrow HH$ subprocess, both in the SM and in the framework of the EChL. In the latter case, we will study how the behaviour of this process is sensitive to the variations of the EChL parameters, checking also whether unitarity might be compromised. In section 4, this analysis will be extended to a whole process that could take place in an e^+e^- collider. First we will extract some results within the SM, comparing MonteCarlo simulations to the effective W approximation (which assumes the W 's are “partons” inside the electrons). Then we will check how the whole process is affected by changes in the EChL parameters, making predictions on the number of events that could be detected. Our conclusions will be shown in section 5.

2 The Electroweak Chiral Lagrangian

Chiral Lagrangians are a powerful tool in order to study the low-energy dynamics of the Goldstone bosons arising from the spontaneous breaking of a particular symmetry. They provide a model-independent treatment of their interactions, being able to parametrize deviations from the SM and allowing direct contact to data. In particular, the Electroweak Chiral Lagrangian is a useful approach to understand the nature of the Goldstone bosons arising from the breaking of the electroweak symmetry and, therefore, to describe the interactions involving W , Z and Higgs bosons. We will first introduce the Chiral Lagrangian in QCD, which is the inspiring refer-

ence for the building of the EChL, and then show how the latter is constructed and how it allows to deal with observables.

2.1 The Chiral Lagrangian in QCD

Chiral Lagrangians were first developed to understand the chiral symmetry breaking in QCD [18]. In the massless limit, strong interactions are invariant under the global transformations:

$$\begin{aligned}\psi_L &\rightarrow L\psi_L, \\ \psi_R &\rightarrow R\psi_R.\end{aligned}\tag{2.1}$$

$\psi_{L(R)}$ are the left- (right-) handed quark fields, and $L(R) \in SU(N_f)_{L(R)}$ are independent rotations, which act respectively on the left- and right-handed fields. N_f is the number of quark flavours which are considered, and could be taken to 6 if all quarks were massless. However, this is not the case. Only the *up* and *down* are light enough (with respect to the natural scale of QCD) to take the massless limit as a good approximation, so the chiral symmetry of QCD is considered to be $SU(2)_L \times SU(2)_R$. In fact, quark mass terms explicitly break chiral symmetry. This explicit breaking is soft if only the two lightest quarks are in the game, not so soft if the strange quark is included as well. The charm, bottom and top quarks are definitely too heavy to even consider the corresponding chiral symmetry at all.

However, the chiral symmetry in QCD is not only explicitly broken by the quark masses, it is also spontaneously broken. The vacuum of QCD (the quark condensate) is not invariant under $SU(2)_L \times SU(2)_R$, and it is only preserved by transformations contained in the subgroup $SU(2)_{L+R}$. According to the Goldstone theorem [10], this SSB will mean the appearance of three degrees of freedom in the form of massless Nambu-Goldstone bosons. As the symmetry is also not exact at the Lagrangian level (due to quark masses), these modes will actually be pseudo-Nambu-Goldstone bosons (pNGB), and will be massive. If only *up* and *down* quarks are considered, three pNGB will arise, which are identified with the three pions. The fact that the explicit breaking of the symmetry is soft is reflected on the small masses of the pions, which are much lighter than the rest of the hadrons. If also the strange quark is considered, the spectrum of pNGBs is enlarged; however, as the strange mass breaks chiral symmetry in a harder way, the masses of these new modes are closer to that of the rest of the hadrons.

The mass difference between the pions and the proton (the lightest among the heavier hadrons) makes it reasonable to write an effective theory which describes the dynamics of these Nambu-Goldstone modes way below the mass of the proton. At these “low energies”, all the other hadrons can be integrated out, as they are too heavy to propagate. Their effect can be taken into account in the values of the couplings which control the interactions between pions.

The next subsection will be dedicated to describing in detail the Chiral Lagrangian in the electroweak theory. As the technical details of the QCD Chiral

Lagrangian are mainly the same as in the electroweak case, they will be omitted here and explained in the following.

2.2 Building the Electroweak Chiral Lagrangian

Chiral Lagrangians can also be applied to the electroweak theory, where a SSB also takes place. As we already showed, the EW sector of the SM is described by a gauge $SU(2)_L \times U(1)_Y$ symmetry, which is exact at the Lagrangian level, but is spontaneously broken due to the presence of a scalar sector. In order to establish a relation to the Chiral Lagrangian, the most convenient form to write the EWSBS Lagrangian is:

$$\mathcal{L}_{\text{SBS}} = \frac{1}{2} \text{Tr}[(D_\mu M)^\dagger (D_\mu M)] - V(M), \quad (2.2)$$

with the potential:

$$V(M) = -\frac{1}{4} \lambda \left[\text{Tr}(M^\dagger M) + \frac{\mu^2}{\lambda} \right]^2. \quad (2.3)$$

M is a matrix which contains all the four real degrees of freedom of the scalar sector:

$$M = \begin{pmatrix} \phi_0^* & \phi^\dagger \\ -\phi^- & \phi_0 \end{pmatrix}. \quad (2.4)$$

The covariant derivative in equation 2.2 only involves the gauge bosons associated to the electroweak group, and clearly not the gluons (as the scalar is a singlet under $SU(3)_C$). The scalar potential has a non-zero minimum when $\mu^2 < 0$ (in fact, infinite non-zero degenerate minima), yielding a non-trivial ground state which is not invariant under the gauge symmetry. Once ϕ_0 takes a vacuum expectation value (vev), this symmetry breaking occurs, and the Higgs boson becomes a propagating mode.

Three NGBs will arise from this SSB. Via the Higgs mechanism, these modes will mix with the electroweak gauge bosons (which are massless before the symmetry is broken), and will constitute the longitudinal degrees of freedom of the latter, rendering them massive. This is how the W and Z bosons acquire masses. The photon stays massless, because, as it has been mentioned, the full electroweak symmetry is not broken and the electromagnetic gauge group is still preserved.

Aside from the gauge electroweak symmetry, the scalar sector also exhibits a global $SU(2)_L \times SU(2)_R$ symmetry (called EW chiral symmetry): the Lagrangian in equation 2.2 stays unchanged under global transformations of the kind:

$$M \rightarrow LMR^\dagger, \quad (2.5)$$

with $L(R) \in SU(2)_{L(R)}$.

However, this symmetry is also broken when ϕ_0 takes a vev: the remaining symmetry is called custodial: $SU(2)_L \times SU(2)_R \rightarrow SU(2)_C = SU(2)_{L+R}$. This subgroup is responsible for the relation between the masses of the W and Z bosons, $M_W = M_Z \cos \theta_W$.

This was a quick summary of the basics of the spontaneous breaking of the electroweak symmetry through the Higgs mechanism. Nevertheless, as it was stated in the introduction, some issues remain unsolved in this sector of the SM. Why is the Higgs mass so small? Why is it the only fundamental scalar in nature? Is it really fundamental, or could it be composite? Is there a bigger symmetry which protects the Higgs mass? Could the Higgs be a pNGB of this symmetry?

Some of the BSM theories which attempt to answer these questions make some predictions on the interactions involving Goldstone/gauge and Higgs bosons [24–27]. Thus, understanding deeply how these particles interact is key to achieving a full knowledge on the true nature of the EWSBS.

So far, experiment seems to be in almost total agreement with the SM, meaning that any New Physics should be observed at energies above our current experimental limits. Nevertheless, some consequences from a hypothetical UV theory could be detected at energies within our reach, as small deviations from the SM predictions. In this sense, effective theories are a perfect tool to probe the EWSBS. They allow to compute observables which can be directly compared to experimental results in a model-independent way, and are able to parametrize deviations from the SM which can afterwards be interpreted in different theoretical frameworks.

In particular, the EChL is an effective theory which describes the dynamics of the electroweak Nambu-Goldstone bosons way below a certain energy scale Λ , that will be discussed shortly. The EChL incorporates the same symmetries as the SM (gauge electroweak and global chiral symmetries) and the same particle content (as all hypothetical heavier particles cannot propagate): the Higgs, Goldstone and gauge bosons. Regarding the fermions, we will assume they have exactly the same interactions as in the SM. Therefore, we will not discuss the fermionic sector in this work.

It is worth noting that, before the Higgs boson was discovered at the LHC in 2012, considerable effort was made employing the Electroweak Chiral Lagrangian in its “Higgsless” version [28–33]. The Higgs boson mass was expected to be considerably larger than it finally turned out to be (some theoretical arguments set upper bounds at hundreds of GeV), so it was considered a heavy field and integrated out. When the Higgs mass was finally set by experiments at 125 GeV, the EChL was modified to include the Higgs boson as a propagating degree of freedom, in the way that will be explained in the following.

The way to introduce these fields in an effective theory is not unique; in fact, many representations are possible, yielding representation dependent Lagrangians. However, physical predictions are obviously representation independent. In the EChL [34], [35], the Higgs h is included as a chiral singlet, while the Goldstone bosons w are placed in a non-linear exponential representation (same as in the QCD Chiral Lagrangian). The gauge fields, W and B , and their corresponding field

strengths are written as usual. Thus, the building blocks of the EChL are:

$$U = \exp\left(\frac{iw^a\tau^a}{v}\right), \quad (2.6)$$

$$\hat{W}_\mu = \frac{g}{2}\vec{W}_\mu\vec{\tau}, \quad (2.7)$$

$$\hat{B}_\mu = \frac{g'}{2}B_\mu\tau^3, \quad (2.8)$$

$$\hat{W}_{\mu\nu} = \partial_\mu\hat{W}_\nu - \partial_\nu\hat{W}_\mu + i[\hat{W}_\mu, \hat{W}_\nu], \quad (2.9)$$

$$\hat{B}_{\mu\nu} = \partial_\mu\hat{B}_\nu - \partial_\nu\hat{B}_\mu. \quad (2.10)$$

Chiral Lagrangians rely on Chiral Perturbation Theory [36, 37], a method based in performing expansions in the quantity p/Λ , where p is the characteristic momentum (or energy) scale of the dynamics.

In the case of QCD, $\Lambda = 4\pi f_\pi$, where $f_\pi = 93$ MeV is the pion decay constant; in the EW case, $\Lambda = 4\pi v \sim 3$ TeV, where v is the mentioned vev of ϕ_0 . This scale is naturally introduced when performing loop computations, and controls the contributions corresponding to quantum corrections. In other words, a quantum correction associated to a process involving n loops would be suppressed by a factor Λ^{-n} . Nevertheless, this scale is not necessarily the cut-off at which the consequences of the hypothetical UV theory would be manifest. For instance, in QCD, $4\pi f_\pi$ does not exactly coincide with the mass of the proton, which is roughly where high-energy dynamics start to be relevant. An effective theory can be trusted if it describes physics way below these two scales (the natural one arising from loops and the UV cut-off).

So far, experiment has ruled out the existence of New Physics: the data obtained at the LHC, where the highest energies are reached, is consistent with the SM. This means the UV cut-off is still unknown, and must be, at least, at the $\mathcal{O}(\text{TeV})$ scale or above. Thus, the natural loop scale, $4\pi v$, marks the limit up to which the EChL can be consistently employed as an effective low-energy theory.

The quotient p/Λ is expected to be small (if it was not, an effective theory would be nonsensical), and, thus, a power series can be written. In Chiral Lagrangians, the different terms that can be written are organized according to their ‘‘chiral dimension’’, which essentially determines the power of p involved in a certain term. The masses and momenta of the fields are of order p . This procedure allows to write the EChL as the sum of different pieces:

$$\mathcal{L}_{\text{EChL}} = \mathcal{L}_{\text{GF}} + \mathcal{L}_{\text{FP}} + \mathcal{L}_2 + \mathcal{L}_4 + \dots \quad (2.11)$$

\mathcal{L}_{GF} and \mathcal{L}_{FP} are, respectively, the gauge-fixing and the non-Abelian Fadeev-Popov terms, while \mathcal{L}_i contains all the terms with chiral dimension i (terms which scale as p^i). The higher order terms will be suppressed by powers of Λ , so they will be subleading.

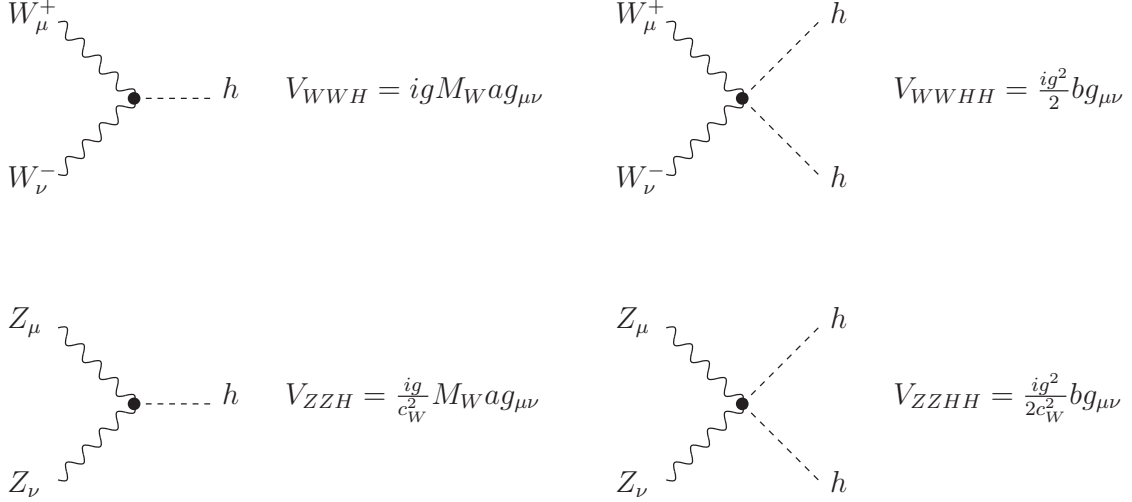


Figure 2.1: Feynman rules extracted from the EChL for Higgs-gauge bosons interactions.

In particular, the first term reads:

$$\begin{aligned}
\mathcal{L}_2 = & -\frac{1}{2g^2} \text{Tr} \left(\hat{W}_{\mu\nu} \hat{W}^{\mu\nu} \right) - \frac{1}{2g'^2} \text{Tr} \left(\hat{B}_{\mu\nu} \hat{B}^{\mu\nu} \right) + \frac{1}{2} \partial_\mu h \partial^\mu h - V(h) + \\
& \frac{v^2}{4} \mathcal{F}(h) \text{Tr} \left(D_\mu U^\dagger D^\mu U \right) + \dots
\end{aligned} \tag{2.12}$$

The covariant derivative of the matrix field U reads:

$$D_\mu U = \partial_\mu U + i\hat{W}_\mu U - iU\hat{B}_\mu. \tag{2.13}$$

As the Higgs field is introduced in the EChL as a chiral singlet, $\mathcal{F}(h)$ can be an arbitrary function. The usual choice is a polynomial one:

$$\mathcal{F}(h) = 1 + 2a \frac{h}{v} + b \frac{h^2}{v^2}, \tag{2.14}$$

where a and b are free parameters. Notice that, in the SM, $a = b = 1$.

Once the exponential in equation 2.6 is expressed as a power series, the last term in equation 2.12 will yield interaction terms between the Goldstone, W , Z and Higgs bosons. In particular, the relevant interactions for the present work are the ones involving the physical gauge bosons and the Higgs boson, which are given in figure 2.1.

2.3 Computing observables using the EChL

These Feynman rules directly involve the parameters a and b , and so will the cross sections for processes which include these vertices. The SM Feynman rules are re-

covered when $a = b = 1$, so any deviations from these values would translate on cross sections which would differ from those predicted by the SM. The goal of this work is to determine quantitatively the sensitivity of certain processes to variations of these two parameters, and predict the value for their cross sections when the parameters depart from their SM values. These results could (hopefully) be checked experimentally, determining if deviations from the SM take place. These possible anomalies in the couplings could then be interpreted in different theoretical frameworks, extracting deep conclusions concerning the true nature of the Higgs boson and the EWSBS. However, this is well beyond the intentions of this work.

Vector Boson Scattering (VBS) processes are very useful in this context. These are 2-to-2 processes, with two vector bosons (W or Z) in the initial state, and two vector or Higgs bosons in the final state. They are directly sensitive to the a and b parameters, and, clearly, offer bigger cross sections in the context of a fermionic accelerator than processes with one or two Higgs bosons in initial states (due to the small Yukawa couplings of the fermions we are able to collide). In particular, this work will be devoted to the analysis of the $W^+W^- \rightarrow HH$ process (instead of other interesting ones, such as $ZZ \rightarrow HH$ for instance) for reasons we will explain further on.

The EChL allows to compute observables for any value of the parameters a and b . However, there are both experimental and theoretical reasons which have already set constraints on them.

Regarding b , recent experimental results have for the first time constrained b to be in the allowed region $b \in [-1.02, 2.71]$ at a 95% confidence level [38]. This parameter controls couplings among two gauge and two Higgs bosons, and thus would require the production of two Higgs bosons at tree-level. There are also theoretical arguments [39] to argue that this parameter must be in the range $b \in [-1, 3]$: otherwise resonances at hundreds of GeV would have been detected at the LHC. This work will (attempt to) show how Vector Boson Scattering processes at e^+e^- colliders can be a very interesting source of information regarding this parameter.

A lot more can already be said about a . This parameter controls the interaction concerning two gauge bosons and one Higgs, making it much easier to be tested experimentally (as the production of a single Higgs is more feasible than that of a pair). The combined measurements of ATLAS and CMS with the LHC Run 1 dataset provide a value of $a = 1.04 \pm 0.05$ [40]. Also, this parameter can be fitted using electroweak precision observables, especially the W mass, due to its small uncertainty. Assuming no New Physics contributions, the fits show that, with a 95% confidence level, $a \in [0.99, 1.06]$ [41, 42]. There are also theoretical reasons that favour $a < 1$ [43], employing positivity arguments. Besides, deviations of a few per mille in the Peskin-Takeuchi parameters would set a in the interval $[0.84, 0.95]$ at the 95% confidence level [44]. All in all, there does not seem to be much room for deviations in a with respect to the Standard Model value, $a = 1$.

On the other hand, both parameters are necessarily constrained by unitarity. As it is characteristic of effective (UV incomplete) theories, the EChL may predict scattering probabilities larger than 1 for some values of the parameters it includes. This depends on the energy at which the studied processes take place, and does not set universal constraints on a and b . Nevertheless, imposing unitarity means, at it will be shown, that none of these parameters can deviate too much from their SM values, in order to guarantee the unitarity of the theory and physically acceptable predictions.

In order to study the unitarity properties of a particular scattering process, a partial wave analysis is an optimal tool. The scattering amplitude of a 2-to-2 process, where the spins of the particles are s_1 to s_4 , can be decomposed as:

$$F_{s_1, s_2, s_3, s_4}(s, \theta, \phi) = 16\pi\kappa \sum_J (2J+1) D_{ss'}^{*J}(\phi, \theta, -\phi) a_{J, s_1, s_2, s_3, s_4}(s), \quad (2.15)$$

where s is the squared center-of-mass energy of the process, θ and ϕ are the polar and azimuthal angles, a_J is the partial wave amplitude associated to a total angular momentum J , $s \equiv s_1 - s_2$, $s' \equiv s_3 - s_4$, and D are the Wigner functions. κ is 1 if the external particles are different and 2 if they are identical.

The orthogonality properties of the Wigner functions allow to write the partial wave amplitudes as:

$$a_{J, s_1, s_2, s_3, s_4}(s) = \frac{1}{32\pi\kappa} \int_{-1}^1 d\cos\theta F_{s_1, s_2, s_3, s_4}(s, \cos\theta) d_{ss'}^J(\cos\theta), \quad (2.16)$$

where $d_{ss'}^J(\cos\theta) = e^{i(s'-s)\phi} D_{ss'}^{*J}(\phi, \theta, -\phi)$.

Unitarity requires the modulus of every partial wave amplitude to be smaller than 1. Imposing this feature up to the energy at which the process is taking place allows to determine within which range of values the parameters a and b can live.

Looking for possible anomalous couplings of gauge and Higgs bosons via deviations in a and b is not the only procedure to look for deviations from the SM employing the EChL. Terms in equation 2.11 with higher chiral dimension than \mathcal{L}_2 or \mathcal{L}_4 would yield other Feynman rules modifying interaction vertices of Z and W bosons, and even allowing couplings which do not exist in the SM, such as the one involving 4 Z s. All these possible deviations are also controlled by other EChL parameters, in a similar manner as it was described for a and b . The analysis that will be performed throughout this work could be done in a similar way, employing different processes, in order to test the sensitivity to the other EChL parameters in \mathcal{L}_4 [45].

This work will only deal with tree-level processes; loop level computations are way beyond our intentions. In this theory, divergences appearing at one-loop order from \mathcal{L}_2 can be absorbed by counterterms in \mathcal{L}_4 . A finite prediction of a scattering amplitude, up to $\mathcal{O}(p^4)$, at one-loop level would be of the generic form $F = F^{(2)} + F^{(4)}$. Here, $F^{(2)}$ is the $\mathcal{O}(p^2)$ contribution, arising from \mathcal{L}_2 at tree-level, while $F^{(4)}$

corresponds to $\mathcal{O}(p^4)$ terms, coming from \mathcal{L}_2 at one-loop level and from \mathcal{L}_4 at tree-level. However, renormalization within the EChL framework is still an open line of research (see, for instance, [46, 47]).

2.4 Linear vs. non-linear representations

So far, we have only introduced the EChL, which is a non-linear effective theory, in the sense that the NGBs are introduced in an exponential matrix (equation 2.6). They transform non-linearly under the EW chiral symmetry $SU(2)_L \times U(1)_Y$, as it can be deduced from the transformation properties of the U matrix:

$$U \rightarrow LUR^\dagger, \quad (2.17)$$

with $L \in SU(2)_L$ and $R \in SU(2)_R$.

Nevertheless, there are many possible representations, which would yield different Lagrangians. As the Physics is representation independent, observables should be the same in any of the possible choices for effective theories. This does not mean that the operators in different Lagrangians, or their physical meaning, can be directly related.

One of the most widely employed representations is the linear one, where the NGBs are introduced in a scalar doublet, along with the Higgs boson, in the same manner as in the SM. In fact, this effective theory is referred to as Standard Model Effective Field Theory (SMEFT). For a review, see, for instance, [48]. The Lagrangian in this representation is:

$$\mathcal{L}_{\text{linear}} = \mathcal{L}_{\text{SM}} + \sum_i \frac{f_i}{\Lambda^2} \mathcal{O}_i^{d=6} + \sum_i \frac{f_i}{\Lambda^4} \mathcal{O}_i^{d=8} + \dots \quad (2.18)$$

In the linear representation, the counting of the operators is the standard one, in terms of canonical dimensions, in contrast to the counting in the non-linear representation (where the counting is done attending to chiral dimensions). This linear effective theory includes the SM, but also all possible higher-dimensional operators which respect the expected symmetries (in the electroweak theory, these would be a global chiral symmetry and a gauge $SU(2)_L \times U(1)_Y$ symmetry). These operators are suppressed by powers of the UV scale Λ .

In the SM there are no higher-dimensional operators (all the coefficients f_i would vanish), so the SMEFT parametrizes deviations from the SM through these operators. This is a first difference with respect to the EChL, where anomalous couplings (controlled by the parameters a and b or others, as it has been previously explained) can be extracted from chiral dimension 2 or 4 operators. This explicitly shows that is impossible to make a 1-to-1 identification between operators in the linear and non-linear representations. The way to make this relation becomes even trickier when considering loops. As we have said, in the non-linear representation, NGB one-loop contributions from \mathcal{L}_2 have the same chiral dimension as \mathcal{L}_4 , in contrast to

the linear representation. As a consequence, the renormalization procedure will be very different in both effective theories.

In the previous subsection we motivated how the EChL is a very useful tool in order to look for deviations from the SM through computations of VBS mediated process. The linear representation would also allow to perform this study, but in a different way. As it has been mentioned, the linear Lagrangian includes no deviations from the SM in canonical dimension 4 operators, so higher-dimensional ones should be considered. All possible operators which modify the couplings between Higgs and vector bosons (up to a certain order) should be taken into account, and their coefficients would have the same physical interpretations as $|a - 1|$ and $|b - 1|$, as they quantify how these couplings depart from those described by the SM. In this sense, we believe the EChL is a more practical tool to compute observables, as a single operator encodes all the information regarding the vertices we are interested in, while the SMEFT requires to employ a considerable number of operators and coefficients.

3 Vector Boson Scattering: $W^+W^- \rightarrow HH$ subprocess

As it has been motivated before, VBS mediated processes allow to directly probe the EChL parameters, in particular, a and b , the ones this work is devoted to deal with. In order to test the sensitivities to both of these parameters in a collider, at least two Higgs bosons must be involved in the process, as the parameter b only plays a role in interactions among two gauge and two Higgs bosons. From a theoretical point of view, any subprocess with 2 gauge and 2 Higgs bosons in the external legs would exhibit all these properties. However, when thinking about a complete process in a collider (either the LHC or a leptonic accelerator), any scenario with a Higgs boson in the initial state would be very suppressed, as the couplings of the Higgs bosons to the colliding fermions are extremely small, and would offer much smaller cross sections than $VV \rightarrow HH$ processes. In particular, $WW \rightarrow HH$ is the best choice, rather than $ZZ \rightarrow HH$. Although the Higgs couples slightly stronger to Z s than to W s (as they are heavier), the WW luminosity is larger than the ZZ one, meaning the probability of radiating two W s from the colliding particles is larger than that of two Z s.

Thus, from now on we will dedicate to the study of the $W^+W^- \rightarrow HH$ process, first at the subprocess level and then in the framework of an e^+e^- collider.

At tree level and in the unitary gauge, four diagrams contribute to the $W^+W^- \rightarrow HH$ subprocess, those in figure 3.1.

The Feynman rules employed in our computations will be extracted from the EChL (figure 2.1). As this Lagrangian does not modify the kinetic terms of the SM,

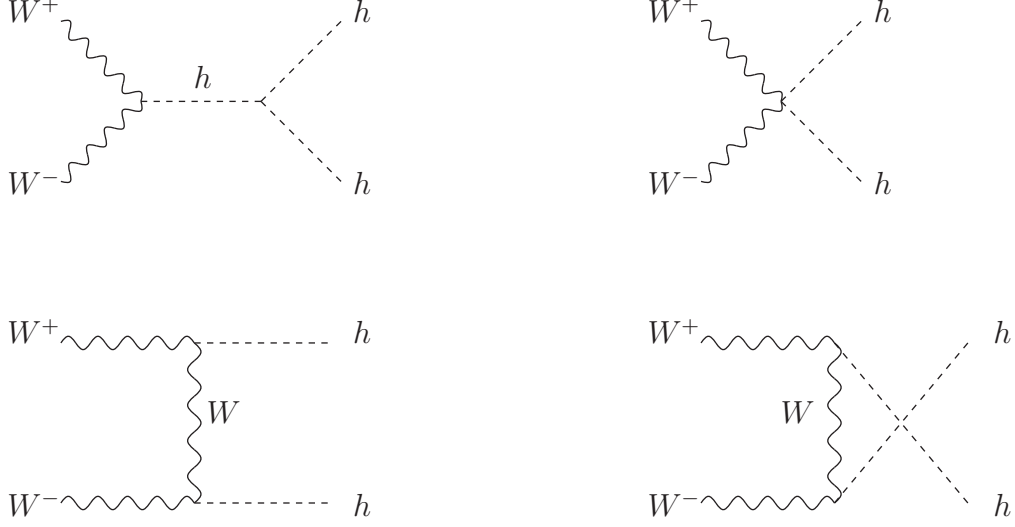


Figure 3.1: Diagrams contributing to the $W^+W^- \rightarrow HH$ subprocess in the unitary gauge.

the only difference with respect to the computation in the SM will be the appearance of the parameters a and b in the couplings between W s and H s. It is worth noting that the EChL allows to modify the Higgs trilinear coupling [49], involved in the s -channel of this process. However, we will set this coupling to its SM value, and only focus on possible deviations from the SM in the WWH and $WWHH$ vertices.

The amplitudes for the different channels (s, t, u and contact channels) are:

$$F_c = \frac{g^2 b}{2} \varepsilon_1 \cdot \varepsilon_2, \quad (3.1)$$

$$F_s = \frac{3g^2 M_H^2 a}{2(s - M_H^2)} \varepsilon_1 \cdot \varepsilon_2, \quad (3.2)$$

$$F_t = \frac{g^2 a^2 M_W^2}{t - M_W^2} \left(\varepsilon_1 \cdot \varepsilon_2 - \frac{(p_t \cdot \varepsilon_1)(p_t \cdot \varepsilon_2)}{M_W^2} \right), \quad (3.3)$$

$$F_u = \frac{g^2 a^2 M_W^2}{u - M_W^2} \left(\varepsilon_1 \cdot \varepsilon_2 - \frac{(p_u \cdot \varepsilon_1)(p_u \cdot \varepsilon_2)}{M_W^2} \right), \quad (3.4)$$

$$F(W^+W^- \rightarrow HH) = F_s + F_u + F_t + F_c, \quad (3.5)$$

where s , t and u are the Mandelstam variables, ε_1 and ε_2 the polarization vectors of the W bosons, g is the weak gauge coupling, and $p_{t(u)}$ is the four-momenta of the virtual W boson propagating in the $t(u)$ -channel.

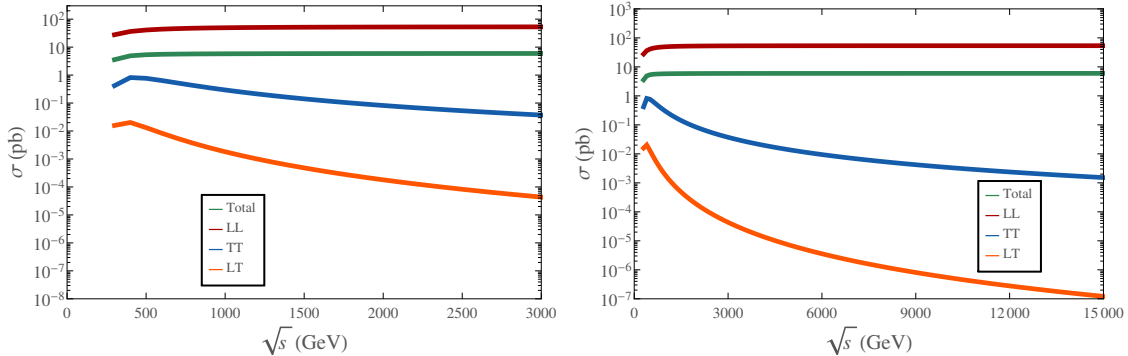


Figure 3.2: Cross sections of the $W^+W^- \rightarrow HH$ subprocess in the SM, as a function of the center-of-mass energy, for all the possible combinations of polarization modes of the W bosons. Left panel shows the predictions up to 3 TeV, while the right one shows them up to 15 TeV.

3.1 SM predictions

First, we believe it is illuminating to analyze how the $W^+W^- \rightarrow HH$ subprocess takes place in the SM. Setting $a = b = 1$ restores the SM Feynman rules.

The cross section in terms of the center-of-mass energy of the subprocess, s , can be computed employing the amplitudes in equations 3.1 to 3.5:

$$\sigma(W^+W^- \rightarrow HH) = \frac{1}{2} \cdot 2\pi \frac{|p_{\text{out}}|}{|p_{\text{in}}|} \frac{1}{64\pi^2 s} \int_{-1}^1 d\cos\theta |\bar{F}|^2(s, \cos\theta). \quad (3.6)$$

The factors 2π and $\frac{1}{2}$ arise, respectively, from the integration over the azimuthal angle and from the fact that two identical particles are produced in the final state. The terms $\frac{|p_{\text{out}}|}{|p_{\text{in}}|} \frac{1}{64\pi^2 s}$ have to do with the phase space, and $|\bar{F}|^2(s, \cos\theta)$ is the squared, spin-averaged scattering amplitude (which is the sum of the four channels).

We will make use of FeynArts 3.10 [50] and FormCalc 9.7 [51] in order to compute the squared, spin-averaged amplitudes and cross sections for this process. The EChL will be implemented employing FeynRules 2.3.32 [52]. Figure 3.2 shows the cross section as a function of the center-of-mass energy (which has a kinematic threshold of $2m_H$), for different polarization modes of the W bosons, longitudinal and transverse. As it could be expected, the longitudinal polarization modes dominate at these energies. Besides, shortly after surpassing the kinematical threshold of $\sqrt{s} = 2m_H$ all dependance of the total cross section with the center-of-mass energy seems to vanish, a characteristic feature of VBS processes.

Regarding unitarity, the s -wave partial amplitude ($J = 0$) will be the dominant one. Figure 3.3 shows the mentioned s -wave amplitude for the different combinations of helicities of the initial W s. These are clearly the only distinct possibilities, since the case where one boson is longitudinally polarized and the other one is transversely polarized vanishes due to parity arguments. None of the amplitudes is bigger than 1 for any energy: this process will never violate unitarity. This is not a surprise at

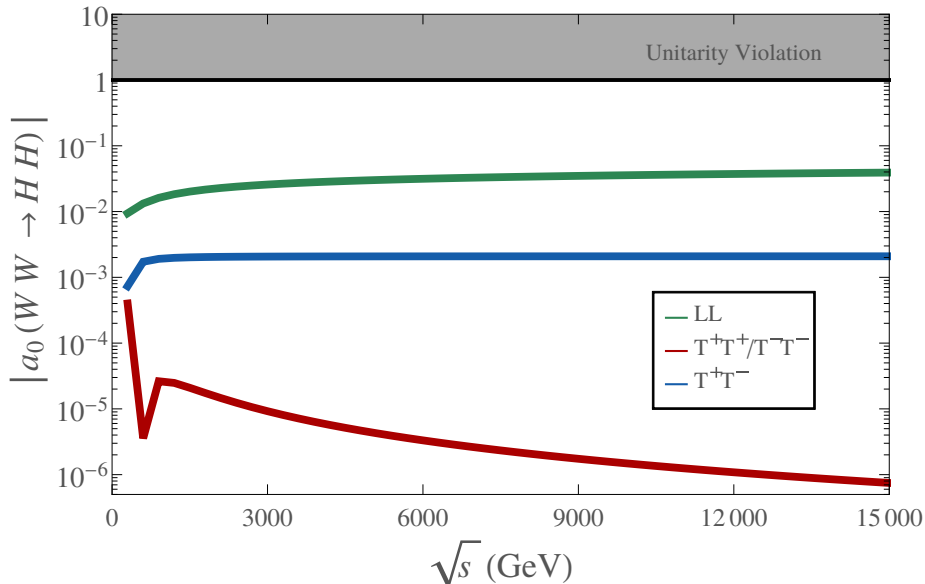


Figure 3.3: Modulus of s -wave partial amplitudes, as a function of the center-of-mass energy, for the $W^+W^- \rightarrow HH$ subprocess in the SM. All combinations of the polarization modes of the initial W bosons which yield a non-vanishing amplitude are shown.

all, as the SM is a unitary Quantum Field Theory.

Summarizing, the $W^+W^- \rightarrow HH$ subprocess does not seem particularly special in the SM. Its total cross section is well behaved with the energy, its dependence being almost flat. There is no problem at all with unitarity, and the longitudinal degrees of freedom of the W bosons provide the biggest contributions to this process.

As a remark, from now on we will not make any further analysis concerning the polarizations of the W bosons. As we will end up embedding the $W^+W^- \rightarrow HH$ subprocess in a complete process that could take place in a collider, it does not make much sense to think of the W s as particles with a particular polarization; they would rather be produced unpolarized, and only the total cross section, summing all modes, is really relevant. Nevertheless, the fact that longitudinally polarizations dominate the cross section allows to control the unitarity behaviour of the total cross section: if the longitudinally polarized s -wave amplitude is smaller than 1, the unitarity of the process will be guaranteed independently of other polarizations and partial wave amplitudes. Thus, from now on we will only compute this particular amplitude when performing unitarity analyses.

3.2 EChL predictions

Figure 3.4 shows how the total cross section of the subprocess depends on the center-of-mass energy when varying the EChL parameters a and b . The values for the parameters are chosen to respect the theoretical constraints (keeping $a \leq 1$). Al-

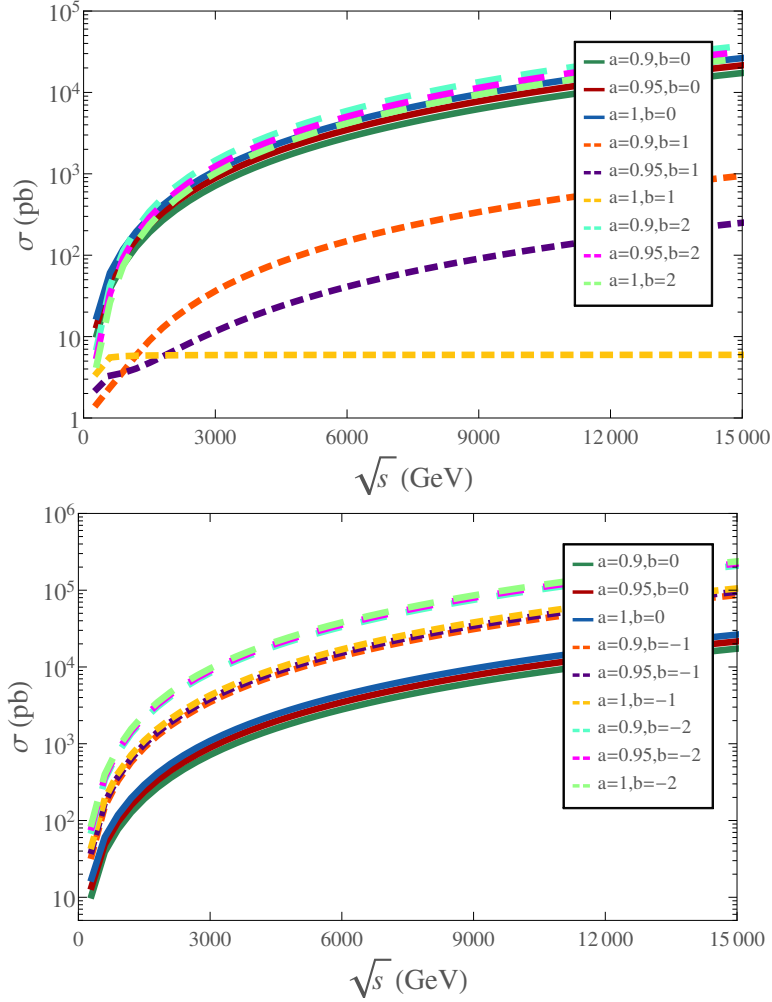


Figure 3.4: Total cross sections of the $W^+W^- \rightarrow HH$ subprocess in the EChL, as a function of the center-of-mass energy, for different values of the parameters a and b . The dashed yellow line corresponds to the SM prediction ($a = b = 1$). Upper panel shows positive values of b whereas lower panel displays negative values.

though some values are slightly outside the experimental bounds, we believe that at this initial stage it is illustrative to show the effects of these parameters when they vary in a wider range.

Some first conclusions can be extracted from these two plots. In figure 3.4 (upper panel), it is plain to see that the behaviour of the cross section is very different from the SM when varying the EChL parameters. While, in the SM case (dashed yellow line), there is hardly any dependence with the energy, in the rest of the cases the cross section grows very steeply. This is not a very nice feature, although it was expected, due to the UV incompleteness of the EChL. These plots also show that, the bigger the deviations of a and b from 1, the bigger the cross section. Thus, some possible New Physics, translated in EChL parameters departing from their SM values, would yield clear experimental evidence, with much larger cross sections than those predicted by the SM. This is yet another advantage of employing this

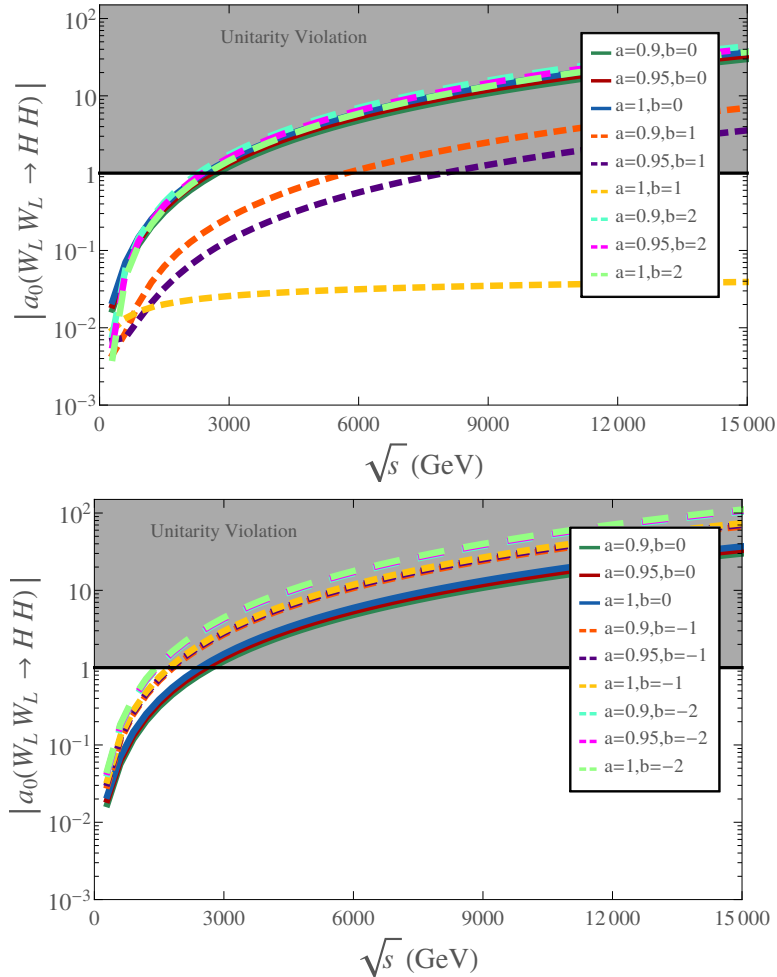


Figure 3.5: Modulus of s -wave partial amplitudes, as a function of the center-of-mass energy, for the $W_L^+ W_L^- \rightarrow HH$ subprocess in the EChL, for different values of the parameters a and b . The dashed yellow line corresponds to the SM prediction ($a = b = 1$). Upper panel shows positive values of b whereas lower panel displays negative values.

type of processes in the quest for New Physics.

It is relevant to note that a possible wrong conclusion can be extracted from these results, especially from 3.4 (lower panel). In this plot, the curves seem to “cluster” in groups of 3, where the curves in each of these groups share a common value of b . This behaviour would lead to the conclusion that it is the parameter b the one that mostly dominates the deviations from the SM. However, this is not so, or at least cannot be confirmed so far. The variations chosen for b with respect to 1 are much bigger than for a , taken into account the good number of theoretical and experimental bounds existing on a , while the constraints are looser for b . In these plots, a varies at most a 10% with respect to 1, and b does so in up to 300%; this very different ranges are responsible for the apparent dominance of b . However, it is not the aim of this section to determine which of the parameters dominates; that will be analyzed in the next section.

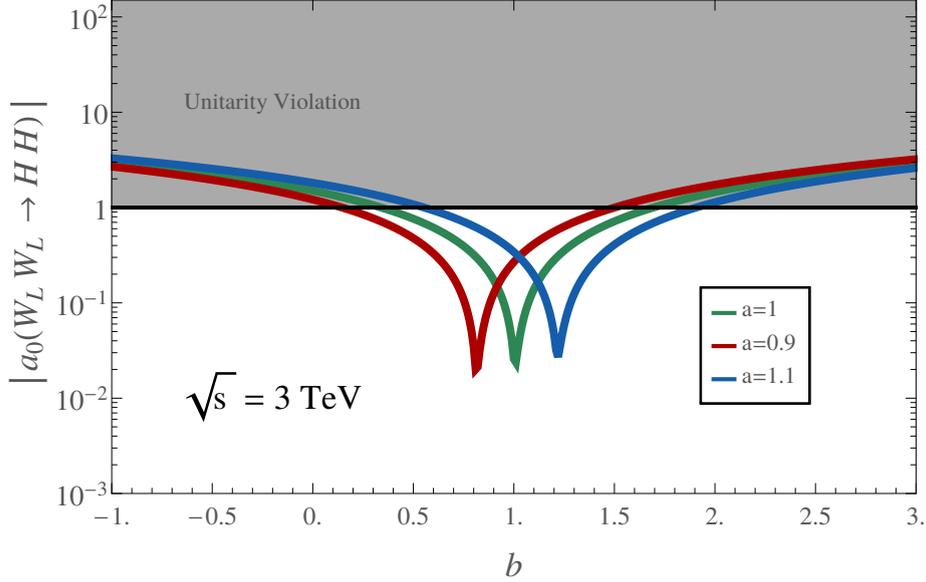


Figure 3.6: In the EChL and at a center-of-mass energy of 3 TeV, modulus of s -wave partial amplitudes for the $W_L^+ W_L^- \rightarrow HH$ subprocess, as a function of the parameter b , for different values of a .

This large increase of the cross sections might indicate that unitarity is not guaranteed: as cross sections are unequivocally related to scattering probabilities, a monotonic growth of the cross section with the energy might mean the probability eventually becomes bigger than 1. In order to check if this problem indeed exists, we will plot, in figure 3.5, the energy dependence of longitudinally polarized s -wave partial amplitude for the same values of a and b . These results show that unitarity is, in fact, a problem. Except in the SM case (which, as it was shown, perfectly respects unitarity), the rest of the chosen values of the parameters render partial wave amplitudes larger than 1 at energies of several TeVs, which could be reachable at colliders. As it could be anticipated, the further from the SM, the sooner unitarity is violated.

Taking into account that the current bounds on a are much more constraining than those on b , it might be interesting to plot the partial wave amplitude, for a fixed energy, as a function of b . Figure 3.6 shows just that, for a fixed energy of 3 TeV, and several values of the parameter a . This is a first attempt at studying how unitarity might be compromised when varying both parameters at once. It can be clearly observed that, at this energy, when a varies from its SM value approximately a 10% (which, roughly speaking, coincides with experimental bounds), b can depart from 1 to 50% at most, in order to obtain physically reasonable predictions.

All in all, these quick results clearly show that the EChL predictions are way different than those of the SM when varying the parameters a and b . Instead of being essentially independent of the center-of-mass energy, the cross section of the $W^+ W^- \rightarrow HH$ process grows with the energy when $a, b \neq 1$, which, although interesting in order to make experimental detections, is problematic in terms of

unitarity. All these effects are enhanced when choosing values of the parameters which differ greatly from those of the SM.

4 Vector Boson Scattering at an e^+e^- accelerator

So far, we have studied the $W^+W^- \rightarrow HH$ subprocess in the framework of the EChL, analyzing how it behaves under variations of the parameters a and b . This preliminary study offers an interesting insight on how the EChL contains very different physics than the SM, as its predictions are both qualitatively and quantitatively different. Nonetheless, the information obtained so far is not really conclusive, as the subprocess alone will never take place. In order to extract solid conclusions, it is necessary to perform a more realistic analysis, and embed the subprocess in a complete process that could take place in a collider.

The first and obvious possibility would be the LHC. It is the most powerful machine available up to date, reaching record center-of-mass energies and luminosities. In fact, there already exist efforts analyzing processes similar to the ones we care about in the context of this accelerator. However, there are some disadvantages in testing VBS processes in the LHC. For starters, statistical studies are really complex. It is necessary to analyze how the vector bosons that start the subprocess are radiated by the quarks that constitute the colliding protons, and then to convolute all this information with the parton distribution functions (PDFs) of the quarks. Due to this “double convolution”, the energy that ends up fueling the $W^+W^- \rightarrow HH$ subprocess will be relatively low, and the cross sections will not be large enough. In fact, the number of events of this kind of process that can be currently achieved does not allow to perform consistent statistical analysis, and thus it is very difficult to obtain solid information about the involved Physics. This is the reason why there is no strong experimental constraint on the b parameter yet, as it is necessary to produce two Higgs bosons to probe it (constraints on a are provided by single Higgs production). Besides, the main decay channel of the Higgs boson is $H \rightarrow b\bar{b}$; each of these quarks would later hadronize, forming jets. As the LHC is a hadronic machine, this type of experimental signature would compete with huge backgrounds, such as those arising from QCD multijet events.

Taking all these considerations into account, we believe that an e^+e^- collider might be the ideal framework in order to study VBS mediated processes and, thus, to probe the EChL parameters. In this kind of machine, the vector bosons would be directly radiated by the colliding leptons (and not from partons of the colliding protons as in the LHC), so it would be easier to transmit a bigger energy to the subprocess. This would be an advantage in order to detect possible anomalous couplings: if a and b were different from 1, this transmission of energy to the subprocess would mean, as it has been shown, an enhancement in the cross section of the subprocess with respect to the SM prediction, meaning more events would be available, a key requirement in order to obtain statistically reliable results. Also, as

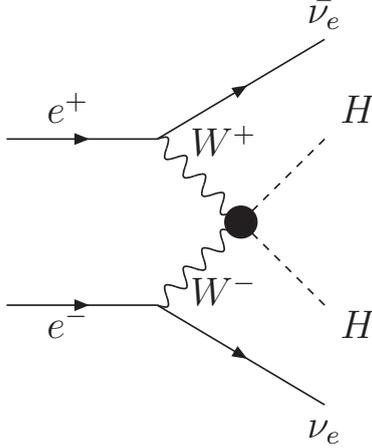


Figure 4.1: Sketch of VBS within an $e^+e^- \rightarrow HH\nu_e\bar{\nu}_e$ process. The black dot generically depicts all diagrams shown in figure 3.1.

this collider involves no hadrons in the initial states, the amount of processes that could produce four jets in the final state would be much smaller, meaning the signal would be much cleaner, and the possible background would not be so relevant.

Currently, there are no leptonic colliders such as the ones we believe could offer very interesting possibilities for this kind of Physics. However, there are prospects for several of these machines to be built in the future. For instance, the International Linear Collider (ILC) [53] aims to reach center-of-mass energies of 250 GeV and, after an update, of even 500 GeV. Also, the Compact Linear Collider (CLIC) [54] is expected to be running at energies of 380 GeV in around 15 years, starting a program of 25-30 years, reaching center-of-mass energies of 3 TeV. We believe this experimental program is encouraging in the search for New Physics: this is the motivation to study VBS mediated processes in the context of an e^+e^- accelerator, hoping our results could be compared to the experimental data once these machines start running.

In this work, we will analyze the $e^+e^- \rightarrow HH\nu_e\bar{\nu}_e$ process: a scenario where each of the colliding leptons radiates a W boson, also producing a neutrino. Both neutrinos would fly away from any detector, meaning a certain energy would be missing. The radiated W s would then scatter, through the subprocess studied in the previous section, producing two Higgs bosons. The VBS contribution to this process is illustrated in figure 4.1.

The aim of this section, and main goal of this work, is to make predictions on how the cross section of this process would depend on the EChL parameters a and b . We will make a scan of the cross section on this two-dimensional parameter space and plot the contour lines. This allows to directly test the sensitivity of the process to the EChL parameters, and is a direct way to detect possible deviations from the SM.

We will make use of the MonteCarlo event generator MadGraph5 [55] in order to make these computations. This software generates events for a certain process, allowing both to compute total cross sections and to obtain differential cross section distributions with respect to several variables. MadGraph allows to implement a certain Particle Physics model, such as the EChL, and to modify its associated parameters (a and b in this case), so it is a powerful tool to check how certain observables depend on them.

Obviously, as Higgs bosons are unstable particles, they will never be detected; only the products of their decays will be. As the main decay channel of the Higgs is to a $b\bar{b}$ pair, the actual whole process would be $e^+e^- \rightarrow \nu_e\bar{\nu}_e b\bar{b}b\bar{b}$. Each of the four quarks would then hadronize, forming b -jets. Thus, the experimental signature of this process would consist on four jets and missing energy (associated to the neutrinos, which cannot be detected).

A study in full glory of the possible experimental detection of the processes we are interested in would require a deeper analysis: performing differential cross section distributions with respect to several kinematical variables, analyzing the possible backgrounds, reconstructing the jets... It is beyond the reach of this work to perform such a careful study.

Nevertheless, we attempt to make some, although approximate, realistic predictions on the experimental consequences on possible deviations from the SM in the VBS processes that have been described. In order to do so, we will employ MadGraph to compute the cross section of the full $e^+e^- \rightarrow \nu_e\bar{\nu}_e b\bar{b}b\bar{b}$ process. This software allows to impose cuts on the final particles. Finally, we will try to make an estimation of the jet reconstruction by introducing a b -tagging efficiency factor. Of course, both the cuts and the tagging efficiency will reduce the cross section. We will make use of the expected luminosities for the future e^+e^- colliders in order to provide quantitative predictions on the number of events. This will be done for several energies (according to the expectations of these future machines) and in the whole (a, b) parameter space.

4.1 The Effective W approximation compared to MC simulations

First, we will try to understand profoundly the Physics involved in the $e^+e^- \rightarrow HH\nu_e\bar{\nu}_e$ process. Although it involves VBS diagrams, such as the ones sketched in figure 4.1, there are some others that would also contribute to the same process. All these diagrams, 32 in total, can be found in appendix A. Diagrams 21 to 24 are the ones which involve VBS (the same as in figure 3.1). Many of the rest involve vertices between Higgs bosons and electrons, and thus could be neglected (as the Yukawa coupling of the electron is really small). However, there are some Z -mediated processes (diagrams 1 to 4) that involve similar couplings to the diagrams involved in the $W^+W^- \rightarrow HH$ subprocess and, thus, could not be neglected a priori.

It is interesting to quantify how relevant VBS diagrams are, as we already understand how these subprocesses are sensitive to the a and b parameters. In order to do so, two strategies can be followed:

- A comparison of the process with electron neutrinos in the final state with a second process with muon neutrinos in the final state provides a good estimate of how relevant the VBS diagrams are. Out of the 32 diagrams that contribute to the $e^+e^- \rightarrow HH\nu_e\bar{\nu}_e$ process, only 12 of them could take place replacing the electron neutrinos with muon neutrinos. Out of the 20 remaining, all involve couplings between Higgs and electrons (which are negligible) except the four VBS diagrams. This means that the difference between the $e^+e^- \rightarrow HH\nu_e\bar{\nu}_e$ and $e^+e^- \rightarrow HH\nu_\mu\bar{\nu}_\mu$ quantifies the weight of the VBS diagrams in the full process. We define the quantity R_{VBS} ,

$$R_{\text{VBS}} = \frac{\sigma(e^+e^- \rightarrow HH\nu_e\bar{\nu}_e) - \sigma(e^+e^- \rightarrow HH\nu_\mu\bar{\nu}_\mu)}{\sigma(e^+e^- \rightarrow HH\nu_e\bar{\nu}_e)}. \quad (4.1)$$

This is an adimensional quantity that clearly determines how large is the contribution of VBS mediated processes to the $e^+e^- \rightarrow HH\nu_e\bar{\nu}_e$ process. If R_{VBS} is close to 1, the cross section will be mostly dominated by VBS. This would be the ideal situation in order to test the sensitivity to the EChL parameters.

The cross sections for both the $e^+e^- \rightarrow HH\nu_e\bar{\nu}_e$ and the $e^+e^- \rightarrow HH\nu_\mu\bar{\nu}_\mu$ processes will be computed employing MadGraph.

We would like to note that R_{VBS} is not a measurable quantity, since it is experimentally impossible to distinguish the flavour of the neutrinos (they all escape the detectors). Besides, the contribution of the subset of diagrams which exhibit VBS configuration is not a physically meaningful quantity, as they are not a gauge invariant subset. Only the whole set of diagrams provides a gauge invariant amplitude and, thus, physically reasonable predictions. Nevertheless, it is useful to understand numerically the relevance of certain subprocesses.

- The effective W approximation (EWA) [56] treats vector bosons as partons inside the fermions, just as quarks and gluons are considered partons inside a proton. This allows to define distribution functions for the vector bosons inside a fermion, in the same way as the PDFs of quarks and gluons inside a proton. The EWA also assumes that the vector bosons are radiated colinearly by the fermions, and then scatter on-shell in the subprocess. This allows to employ factorization, obtaining the cross section for the whole process by convoluting that of the subprocess with the ‘‘PDFs’’ of the vector bosons:

$$\sigma_T(s) = \int dx_1 \int dx_2 f(x_1) f(x_2) \hat{\sigma}(\hat{s}). \quad (4.2)$$

Here, $\sigma_T(s) \equiv \sigma(e^+e^- \rightarrow HH\nu_e\bar{\nu}_e)$ is the total cross section for the complete process taking place at a center-of-mass energy of \sqrt{s} ; $\hat{\sigma}(\hat{s}) \equiv \sigma(W^+W^- \rightarrow HH)$ is the cross section for the subprocess at a center-of-mass energy of $\hat{s} = x_1x_2s$; x_1 and x_2 are the fractions of the momentum of the electrons carried

by the two vector bosons respectively; and $f(x_1)$ and $f(x_2)$ their distribution functions.

In practice, this double integral is really a triple one. The squared scattering amplitude is directly related to the differential cross section with respect to the polar angle; obtaining the cross section of the subprocess involves an integration over this variable, which needs to be performed along with the ones over x_1 and x_2 . It is absolutely impractical to compute these integrations analytically: we will solve them numerically employing Vegas [57], a Monte Carlo integration software. The details of our computation can be seen in appendix B.

A key point about the EWA is the fact that the ‘‘PDFs’’ of the vector bosons are different for longitudinally and transversely polarized bosons. This means that equation 4.2 is actually more complicated:

$$\sigma_T(s) = \int dx_1 \int dx_2 \sum_{ij} f_i(x_1) f_j(x_2) \hat{\sigma}_{ij}(\hat{s}). \quad (4.3)$$

The indices i and j run over the longitudinal and transverse polarizations. $\hat{\sigma}_{ij}(\hat{s})$ is the cross section for the subprocess where the initial vector bosons have polarizations i and j respectively. The cross sections for the different polarizations will be taken from those computed in the analysis of the subprocess. Regarding the distribution functions of the vector bosons, there has been a considerable effort in the literature on trying to find the optimal choice [56, 58, 59]. [56] provides the distribution functions in two ways. One of them assumes the energy E of the fermions which ‘‘contain’’ the vector bosons is much larger than the mass of the latter, M_W , obtaining simple expressions employing the so-called Leading Log Approximation (LLA), which applies in this limit, $E \gg M_W$. The improved formulas go beyond the LLA, also keeping terms of order M_W^2/E^2 , rendering more complicated expressions. We will employ these two versions of the distribution functions and compare their results.

Due to the intrinsic nature of the EWA, it implies that VBS processes are the most relevant contribution to the complete process. A comparison of the results obtained employing this method with the full ones obtained from MadGraph can also provide an insight on how relevant the contribution from VBS actually is.

Table 4.1 shows the values of the cross sections, in picobarns, for different scenarios. The first line shows the values for the $e^+e^- \rightarrow HH\nu_e\bar{\nu}_e$ process computed by MadGraph. As it has been mentioned, this cross section gets contributions from VBS diagrams, but also from other type of diagrams, so, a priori, it is unclear how relevant VBS actually is. The second and third lines contain the results obtained employing the EWA, using both the approximate and improved vector boson PDFs. As we have mentioned, both these sets of cross sections only get VBS contributions. Finally, the last line shows the cross section for the $e^+e^- \rightarrow HH\nu_\mu\bar{\nu}_\mu$ process, which

\sqrt{s} (TeV)	0.5	1	2	3
MadGraph	$1.3 \cdot 10^{-5}$	$8.0 \cdot 10^{-5}$	$4.0 \cdot 10^{-4}$	$8.0 \cdot 10^{-4}$
LLA EWA	$2.8 \cdot 10^{-5}$	$3.7 \cdot 10^{-4}$	$1.5 \cdot 10^{-3}$	$2.8 \cdot 10^{-3}$
Improved EWA	$7.7 \cdot 10^{-6}$	$1.2 \cdot 10^{-4}$	$4.8 \cdot 10^{-4}$	$8.5 \cdot 10^{-4}$
MadGraph with ν_μ	$1.0 \cdot 10^{-5}$	$8.1 \cdot 10^{-6}$	$3.7 \cdot 10^{-6}$	$2.2 \cdot 10^{-6}$

Table 4.1: Cross sections (in pb) in the SM, for different center-of-mass energies, computed employing various methods.

essentially gets the same contributions as that with electron neutrinos in the final state, but removing all which come from VBS. All those values are computed for several center-of-mass energies, and within the SM ($a = b = 1$).

Table 4.2 is much more illuminating. It shows the ratio between the cross sections for the $e^+e^- \rightarrow HH\nu_e\bar{\nu}_e$ process computed via the EWA and via MadGraph. Its last line contains the value of the coefficient R_{VBS} , defined in equation 4.1, which quantifies the relevance of the vector boson scattering diagrams. Clear conclusions can be extracted from these results. For starters, the effective W approximation tends to overestimate the value of the cross section, so there will probably exist some destructive interference between VBS diagrams and those which do not involve this type of subprocesses. Besides, as it can be expected, as R_{VBS} approaches 1, so does the ratio between the EWA and MadGraph values. This is totally reasonable: the more important VBS is, the more accurate the EWA is. This behaviour is enhanced for higher energies; in fact, the EWA is an excellent approach to perform these computations above 1 TeV. These results also confirm that the expressions obtained within the LLA for the vector bosons distribution functions are not optimal. Although they also provide better results when increasing the energy of the process, they do not quite mimic the values obtained with MadGraph, while the improved formulas do.

It is also interesting to analyze the behaviour of the differential cross section with respect to M_{HH} , the invariant mass of the Higgs pair. MadGraph provides all the kinematical information for each simulated event, and thus directly allows to plot distributions. These can be compared to the results obtained employing the

\sqrt{s} (TeV)	0.5	1	2	3
LLA EWA	2.19	4.59	3.78	3.34
Improved EWA	0.59	1.48	1.2	1.06
R_{VBS}	0.3	0.9	0.99	0.997

Table 4.2: Within the SM, quantifications of the relevance of the VBS contribution in the whole $e^+e^- \rightarrow HH\nu_e\bar{\nu}_e$ process for different center-of-mass energies. The first two lines include the ratios of the cross sections compared via the EWA and via MadGraph. The last line shows the value of the coefficient R_{VBS} , defined in equation 4.1.

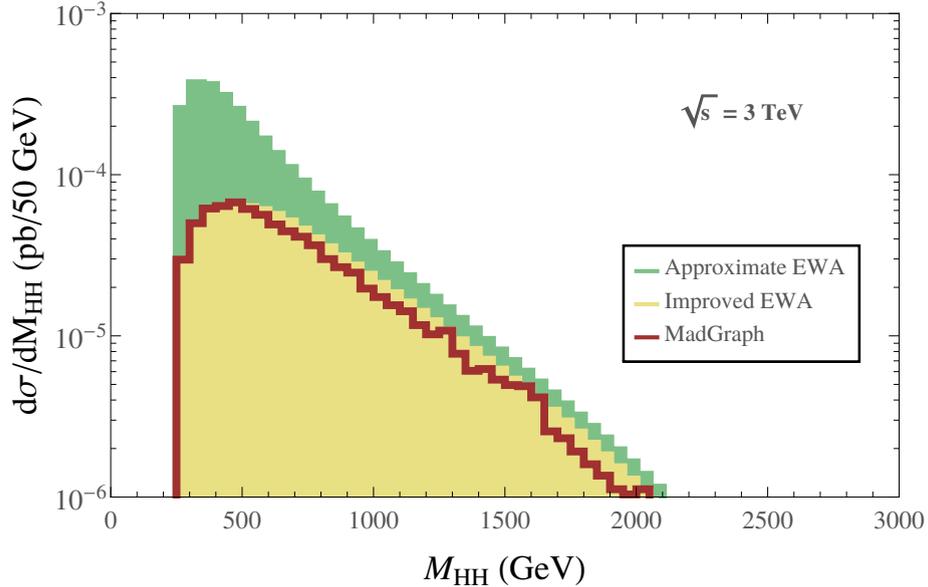


Figure 4.2: In the SM, predictions for the behaviour of the $e^+e^- \rightarrow HH\nu_e\bar{\nu}_e$ cross section distribution with respect to the Higgs pair invariant mass, M_{HH} .

EWA. This information is shown in figure 4.2, which includes the results obtained employing both methods for a center-of-mass energy of 3 TeV (in the case of the EWA, using both the LLA and the improved distribution functions).

This plot confirms the conclusions that the total cross sections results pointed to. In general, the effective W approximation tends to overestimate the cross section. However, at high energies, it is an excellent approximation, and the functional dependance is reproduced with high accuracy. It is also confirmed that in order to obtain precise results employing the EWA, the improved expressions of the distribution functions need to be employed. The LLA ones are proven to be accurate at high energies (in fact, over 1 TeV they behave very similarly to the improved expressions), but greatly overestimate the cross section at low energies. This explains why the total cross section provided by the approximate distribution functions is several times larger than that obtained with the improved expressions.

All in all, these procedures have yielded an interesting insight on the full $e^+e^- \rightarrow HH\nu_e\bar{\nu}_e$ process within the SM. Apart from many diagrams where the Higgs bosons couple to electrons (which can be neglected), the main contributions are VBS mediated processes or Z mediated processes. Both the EWA and the comparison with the $e^+e^- \rightarrow HH\nu_\mu\bar{\nu}_\mu$ process confirm that, above the TeV, VBS clearly dominates. This could be expected, as the Z mediated diagrams involve one or more Z bosons propagating in an s -channel, and thus decrease with the center-of-mass energy. Besides, it has also been learnt that the EWA constitutes an excellent tool to make computations for this kind of processes, especially at high energies. Nevertheless, the improved expressions for the distribution functions of the vector bosons need to be employed in order to obtain quantitatively accurate results.

	\sqrt{s} (TeV)	0.5	1	2	3
$a = 1.5, b = 1$	MadGraph	$1.2 \cdot 10^{-4}$	$2.4 \cdot 10^{-3}$	$1.5 \cdot 10^{-2}$	$3.6 \cdot 10^{-2}$
	LLA EWA	$4.1 \cdot 10^{-4}$	$5.7 \cdot 10^{-3}$	$2.7 \cdot 10^{-2}$	$5.6 \cdot 10^{-2}$
	Improved EWA	$1.4 \cdot 10^{-4}$	$2.6 \cdot 10^{-3}$	$1.4 \cdot 10^{-2}$	$3.2 \cdot 10^{-2}$
	MadGraph with ν_μ	$2 \cdot 10^{-5}$	$1.9 \cdot 10^{-5}$	$1.9 \cdot 10^{-5}$	$1.9 \cdot 10^{-5}$
$a = 0.5, b = 1$	MadGraph	$1.5 \cdot 10^{-5}$	$3 \cdot 10^{-4}$	0.0026	0.0071
	LLA EWA	$4.9 \cdot 10^{-5}$	$6 \cdot 10^{-4}$	0.0037	0.0089
	Improved EWA	$7.9 \cdot 10^{-6}$	$2 \cdot 10^{-4}$	0.002	0.0058
	MadGraph with ν_μ	$5.2 \cdot 10^{-6}$	$7.7 \cdot 10^{-6}$	$6.9 \cdot 10^{-6}$	$6.5 \cdot 10^{-6}$
$a = 1, b = 1.5$	MadGraph	$1.7 \cdot 10^{-5}$	$9 \cdot 10^{-5}$	$7.9 \cdot 10^{-4}$	$2.4 \cdot 10^{-3}$
	LLA EWA	$3.4 \cdot 10^{-5}$	$3.9 \cdot 10^{-4}$	$2 \cdot 10^{-3}$	$4.5 \cdot 10^{-3}$
	Improved EWA	$2.7 \cdot 10^{-6}$	$6.6 \cdot 10^{-5}$	$6.5 \cdot 10^{-4}$	$2 \cdot 10^{-3}$
	MadGraph with ν_μ	$1.6 \cdot 10^{-5}$	$1.5 \cdot 10^{-5}$	$8.5 \cdot 10^{-6}$	$6.1 \cdot 10^{-6}$
$a = 1, b = 0.5$	MadGraph	$1.7 \cdot 10^{-5}$	$3.3 \cdot 10^{-4}$	$2.3 \cdot 10^{-3}$	$5.5 \cdot 10^{-3}$
	LLA EWA	$5.5 \cdot 10^{-5}$	$8.4 \cdot 10^{-4}$	$4.1 \cdot 10^{-3}$	$8.6 \cdot 10^{-3}$
	Improved EWA	$2 \cdot 10^{-5}$	$3.8 \cdot 10^{-4}$	$2.2 \cdot 10^{-3}$	$5 \cdot 10^{-3}$
	MadGraph with ν_μ	$5.7 \cdot 10^{-6}$	$4.1 \cdot 10^{-6}$	$3.3 \cdot 10^{-6}$	$3.1 \cdot 10^{-6}$

Table 4.3: Predictions of the EChL for the cross sections (in pb), for different values of the parameters a and b and e^+e^- center-of-mass energies, computed employing various methods.

4.2 Sensitivity to the EChL parameters

From now on, we will depart from the SM and analyze how the $e^+e^- \rightarrow HH\nu_e\bar{\nu}_e$ process is affected when the EChL parameters a and b differ from 1. As we showed in section 3, the VBS subprocess cross section is greatly increased when these parameters take values different from 1. Thus, it could be expected that, when modifying them, the contribution of VBS to the total cross section will be even bigger than in the SM. Nevertheless, this is just a naive conclusion. The Z mediated processes (diagrams 1 to 4 in appendix A) also involve vertices among gauge and Higgs bosons which are, of course, controlled by a and b , so it is unclear if the energetic dependance of the full process will resemble that of the SM even when the EChL depart from their SM values.

In order to get a first intuition, we will perform the same analysis as the one that was developed for the SM, but with several values of a and b . Only one parameter will be modified at a time, while the other will be chosen to take values of 0.5 and 1.5. These values are not very consistent, especially for a (they are outside the current experimental constraints, and picking $a > 1$ is theoretically not well motivated). Besides, according to figures 3.5 and 3.6, unitarity might be an issue for this values.

	\sqrt{s} (TeV)	0.5	1	2	3
a=1.5, b=1	LLA EWA	3.4	2.38	1.8	1.56
	Improved EWA	1.17	1.08	0.93	0.89
	R_{VBS}	0.83	0.9921	0.9987	0.99947
a=0.5, b=1	LLA EWA	3.27	2	1.42	1.25
	Improved EWA	0.53	0.67	0.77	0.82
	R_{VBS}	0.65	0.9975	0.9973	0.99985
a=1, b=1.5	LLA EWA	2	4.33	2.53	1.88
	Improved EWA	0.16	0.73	0.82	0.83
	R_{VBS}	0.06	0.83	0.99	0.9975
a=1, b=0.5	LLA EWA	3.24	2.55	1.78	1.56
	Improved EWA	1.18	1.15	0.96	0.91
	R_{VBS}	0.66	0.988	0.9986	0.99944

Table 4.4: Within the EChL, and for different values of the parameters a and b , quantifications of the relevance of the VBS contribution in the whole $e^+e^- \rightarrow HH\nu_e\bar{\nu}_e$ process for different center-of-mass energies. The first two lines include the ratios of the cross sections compared via the EWA and via MadGraph. The last line shows the value of the coefficient R_{VBS} , defined in equation 4.1.

Nonetheless, here we just choose them as some illustrative examples to show the main features of the departures from the SM predictions. The results are shown in figure 4.3 and tables 4.3 and 4.4. As a remark, the distribution plots do not include the results obtained employing the approximate distribution functions in the EWA, as it has been confirmed that the improved expressions provide much better results.

Some information can be extracted from these results. As it was expectable, when a and b are different from 1, vector boson scattering processes tend to dominate, even at lower energies. Thus, in these cases the effective W approximation is even more robust than in the SM case. In fact, the distributions obtained via MadGraph and via the EWA are almost identical, except some differences at low energies, where VBS processes are not so dominant.

Also, it is clear that the results are not the same for symmetric variations of the parameters with respect to the SM: with constant $|a - 1|$ or $|b - 1|$, the behaviour is quantitatively different if the parameters are larger or smaller than 1. In fact, it seems that cross sections tend to grow faster when a is larger than 1 (a scenario that, we insist, is theoretically disfavoured) and when b is smaller than 1.

Besides, now both parameters have been modified in the same ranges, so it is possible to try and take a hint on which of them is more dominant. It seems that the role of a is more important than that of b : cross sections are larger when b is kept to 1 and a varies rather than viceversa. This could be expected a priori. In

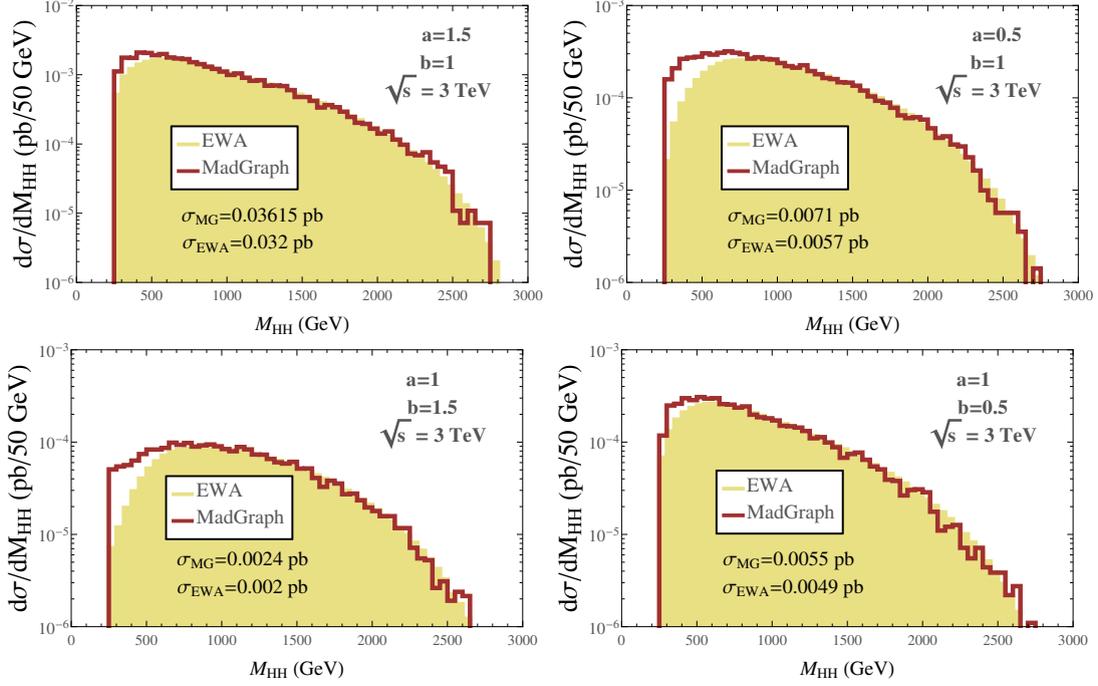


Figure 4.3: In the EChL, and for different values of the parameters a and b , predictions for the behaviour of the $e^+e^- \rightarrow HH\nu_e\bar{\nu}_e$ cross section distribution with respect to the Higgs pair invariant mass, M_{HH} .

the $W^+W^- \rightarrow HH$ process, t - and u -channels involve two vertices between two W s and one Higgs boson. Each of these vertices is controlled by the parameter a , so the scattering amplitude will scale as a^2 . On the other hand, there is only one vertex involving two W s and two Higgses, so the amplitude will scale linearly with b . This can explain why a particular variation in a yields bigger cross sections than the same variation in b .

Nevertheless, these are just some preliminary results to understand how the cross section of the full $e^+e^- \rightarrow HH\nu_e\bar{\nu}_e$ process depend on a and b . Confirming our hypothesis, VBS is even more dominant when a and b depart from their SM values, which implies a higher accuracy when employing the EWA. In this case, the dependance on a and b of the cross section of the whole $e^+e^- \rightarrow HH\nu_e\bar{\nu}_e$ process will essentially be inherited from that of the $W^+W^- \rightarrow HH$ subprocess. Although some diagrams which do not exhibit VBS configuration also depend on a and b , when these parameters depart from 1 their contribution will be much smaller, as VBS dominates.

However, in order to extract solid conclusions, keeping one parameter at 1 and then varying the other is not enough: it is necessary to analyze how the cross section behaves when both parameters are modified. We will perform a scan on the (a, b) two-dimensional parameter space to determine more exactly the behaviour of the process when varying both parameters at once. In order to that, it is necessary to decide the region of the parameter space that will be scanned.

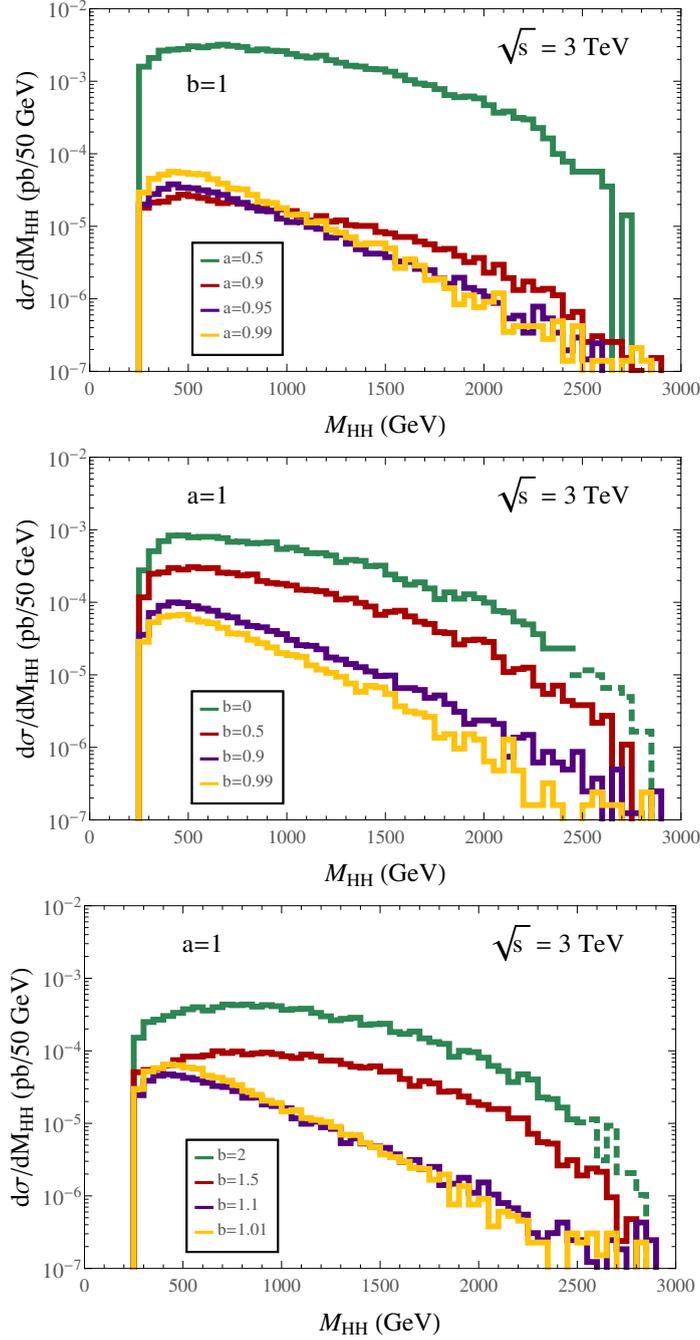


Figure 4.4: In the EChL, and for different values of the parameters a and b , predictions for the behaviour of the $e^+e^- \rightarrow HH\nu_e\bar{\nu}_e$ cross section distribution with respect to the Higgs pair invariant mass, M_{HH} . The center-of-mass energy is set at 3 TeV.

Taking into account that this work attempts to make some realistic predictions in the context of future e^+e^- colliders, it would not be consistent to pick arbitrary values of the EChL parameters. Apart from the current experimental and theoretical bounds, it is necessary to take into account the unitarity analysis. As it was mentioned, the EChL is not a UV complete theory, and choosing certain values for

its parameters might cause scattering probabilities to be larger than 1 when the energy of the process is above a particular threshold. Over this threshold, the EChL is not predictive anymore. A different point of view can be adopted: in a collider, as the energy is fixed, imposing unitarity means that a and b are restricted to a certain range, outside of which the EChL cannot be trusted.

It is possible to make a connection between the process and the subprocess, taking into account that the invariant mass of the Higgs pair, M_{HH} , coincides with the center-of-mass energy of the subprocess. Thus, an analysis of the behaviour of the full e^+e^- process with respect to M_{HH} allows to check if, given certain values for a and b , unitarity is endangered.

Figure 4.4 shows the distributions for different values of a and b . Dashed lines cover regions of M_{HH} where the modulus of the s -wave partial amplitude is larger than 1. These results are consistent with figure 3.5: at around 2.5 TeV, unitarity is violated when b varies from its SM value in around a 50%. Thus, it can be concluded that $b \in [0.5, 1.5]$ is an adequate range for this parameter in order to guarantee unitarity in the framework of the e^+e^- colliders we are interested in.

With these bounds in mind it is possible to perform a scan on the (a, b) parameter space. Figure 4.5 shows the cross section contour lines, obtained with MadGraph, for energies of 500 GeV, 1 TeV and 3 TeV.

The ranges for the parameters have been chosen such that unitarity is guaranteed within the considered parameter space. Although the range for a is larger than the one it is actually constrained to, we wanted to display the same ranges for both parameters in order to obtain a global view. The dotted region is theoretically disfavoured by positivity, while the orange one contains the experimentally allowed region for a , within a 95% confidence level.

These plots finally provide solid conclusions on the sensitivity of the $e^+e^- \rightarrow HH\nu_e\bar{\nu}_e$ process to variations of the EChL parameters. As both a and b are modified simultaneously and in the same range, it is possible to compare their role on the behaviour of the cross section.

For starters, it is clear that the plots are not symmetrical with respect to the (1,1) point, which means that increasing any of the parameters with respect to 1 in a certain amount is not equivalent to diminishing it in the same amount. This happens for both parameters: the plots do not exhibit any symmetry with respect to the $a = 1$ or $b = 1$ axes. This means that the cross section is sensitive to the sign of $a - 1$ and $b - 1$. This was already observed in figure 4.3, and is now confirmed. This can be understood diagrammatically. A quick look at appendix A shows that the $e^+e^- \rightarrow HH\nu_e\bar{\nu}_e$ process gets contributions from diagrams with one vertex between one Higgs and two gauge bosons (which scale as a), diagrams with two of these vertices (proportional to a^2) and diagrams with interactions among two Higgs and two gauge bosons (scaling as b). This means that the scattering amplitude can be

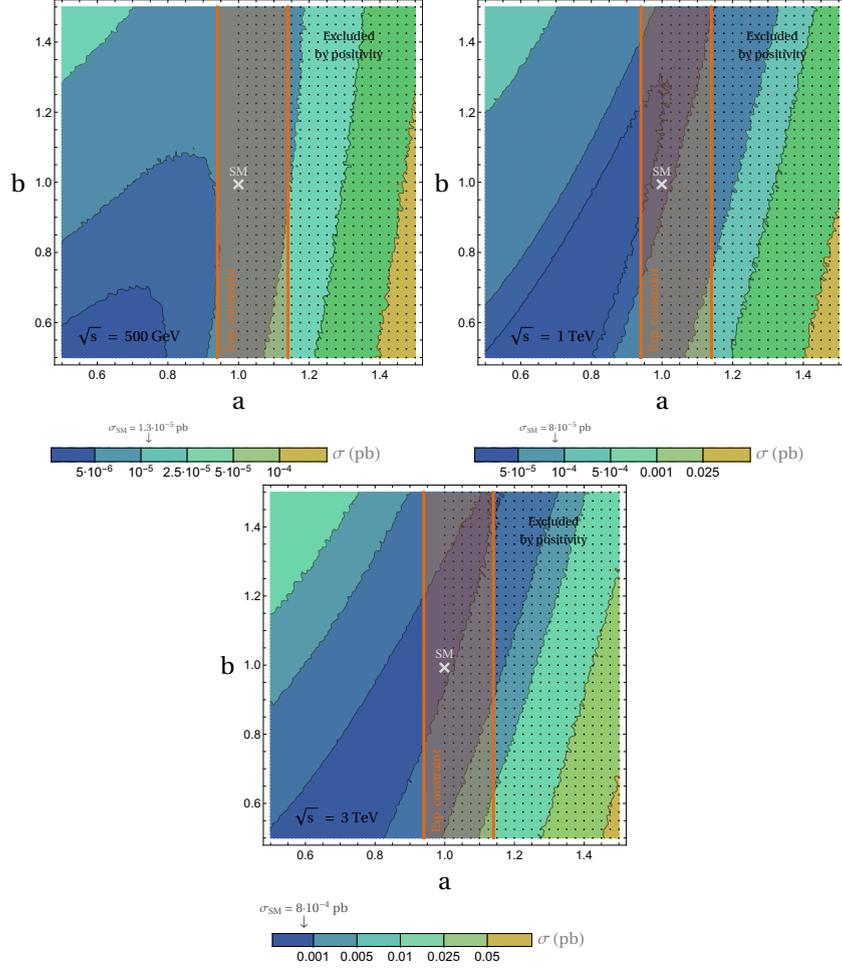


Figure 4.5: EChL predictions for contour lines of $\sigma(e^+e^- \rightarrow HH\nu_e\bar{\nu}_e)$ (in pb) in the (a, b) parameter space, at a center-of-mass energy of 500 GeV (upper panel), 1 TeV (middle panel) and 3 TeV (lower panel). The dotted region is excluded by positivity, while the orange one shows the experimentally allowed region for a . The white cross represents the SM prediction ($a = b = 1$).

written as:

$$F = \alpha a^2 + \beta b + \gamma a, \quad (4.4)$$

where α , β and γ are coefficients which do not depend on the EChL parameters, and will depend on the relevant kinematical variables. As it was already mentioned, the dependence of the amplitude on a and b will be essentially inherited from the subprocess (equations 3.1 to 3.5) when VBS is sufficiently dominant (practically in all the parameter space).

The difference with respect to the SM can be written as:

$$F - F_{\text{SM}} = \alpha(a^2 - 1) + \beta(b - 1) + \gamma(a - 1). \quad (4.5)$$

When squaring this amplitude in order to compute cross sections, the interferences between the three pieces will definitely be sensitive to the signs of $a - 1$, $b - 1$ and

$a^2 - 1$. This can explain why deviations from the SM are not symmetric with respect to its values for a and b .

Also, the plots are not symmetrical with respect to the $a = b$ line: equal variations in a and b are not equivalent. Clearly a is the dominant parameter: cross sections grow faster when keeping b constant and varying a than viceversa. This could also be expected due to the quadratic dependance on a in equation 4.4, and could offer some insight on the coefficients α , β and γ , although we will not focus on them.

When comparing the three plots, it is also clear that the behaviour of the cross section with respect to the EChL parameters is sensitive to the energy of the process: the shape of the contour lines is modified when increasing the energy. At 500 GeV, some sort of closed ellipses can be glimpsed, but at higher energies these ellipses start stretching, and even opening at 3 TeV. This means that the functional dependance of the cross section with respect to both parameters varies with the energy of the process. This can be translated in different energetic dependances of the parameters α , β and γ , which can be understood in terms of diagrams. For instance, diagrams that scale linearly with a (diagrams 1 and 24 in appendix A) involve Z or Higgs bosons propagating in an s -channel, and, thus, will decrease with the energy: so will the coefficient γ . On the other hand, diagrams which are quadratic in a or linear in b will involve, among others, VBS processes, which are enhanced as the energy of the process increases. All in all, the relative relevance of the coefficients α , β and γ depends on the energy, being the latter the most suppressed at high energies. This is translated in different functional dependances in the cross section, and, therefore, in the changes of the shapes of the ellipses, as the plots confirm.

Comparing these results to the ones obtained previously, especially in section 3, there appears to be a contradiction. The cross section of the subprocess increased considerably with respect to the SM predictions when a and/or b differed from 1. However, in the contour plots displayed for 500 GeV and 1 TeV, it is clear than there is a region of the parameter space where the cross section is smaller than the SM value, especially at 500 GeV. This is no contradiction at all: when the relevance of the VBS contribution was quantified in subsection 4.1, we learnt that, at low energies, these processes were not the dominant ones. This explains why, although VBS is enhanced when a and b depart from 1, the cross section of the full process may not. In order to make a quantitative analysis of this feature, it would be necessary to study in depth how the dynamics of Z mediated processes behave when varying the EChL parameters. This is beyond our intentions. However, at higher energies, the SM lies within the region with the smallest cross section, as it could be expected (at this energy, the VBS contribution is hugely dominant).

The conclusions obtained so far provide interesting information on how the EChL parameters control the behaviour of the $e^+e^- \rightarrow HH\nu_e\bar{\nu}_e$ process. Nevertheless, in order to obtain experimentally testable results, it is necessary to analyze a final state where the Higgs bosons have decayed. We will choose its main decay channel, $H \rightarrow b\bar{b}$, yielding a final state with four jets (due to the hadronization of the quarks) and missing energy (associated to the neutrinos). As it has been argued, the analysis

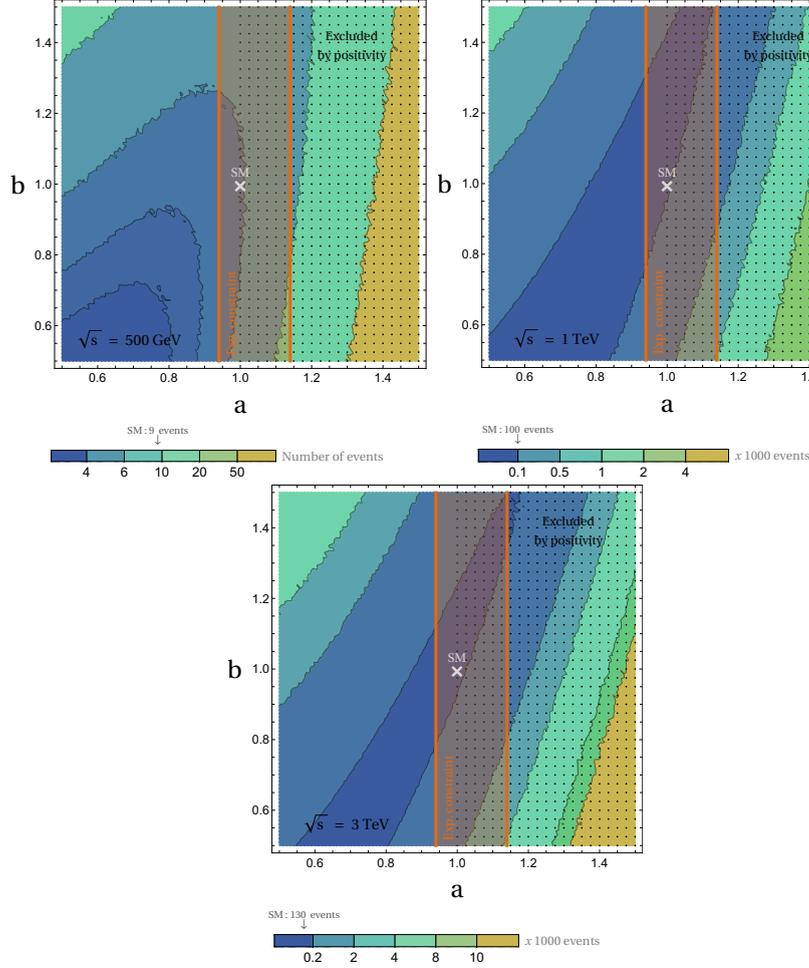


Figure 4.6: EChL predictions for contour lines of number of events of the full process, $e^+e^- \rightarrow HH\nu_e\bar{\nu}_e \rightarrow b\bar{b}b\bar{b}\nu_e\bar{\nu}_e$, in the (a, b) parameter space after the cuts shown in equation 4.6 are applied, at a center-of-mass energy of 500 GeV (upper panel), 1 TeV (middle panel) and 3 TeV (lower panel). The dotted region is excluded by positivity, while the orange one shows the experimentally allowed region for a . The white cross represents the SM prediction ($a = b = 1$).

of this final state is not trivial at all, so we just aim to obtain an estimation. In order to do so, we will perform a Monte Carlo simulation employing MadGraph: the same computation that was already worked out, but including the decays of the Higgs bosons. We will implement some cuts to the final particles, in order to ensure their detection. Jets with low transverse momentum cannot be detected. On the other hand, it is expectable that the neutrinos carry a non-negligible fraction of the energy of the incoming electrons. These considerations imply to require a minimum missing energy \cancel{E}_T and a minimum transverse momenta p_T^j for the jets. Besides, in order not to lose signal in the direction of the beams, a cut in the polar angle θ is needed. Equivalently, a maximum pseudorapidity $\eta^j \equiv -\log(\tan \frac{\theta}{2})$ for the jets is established. Finally, in order to be detectable, the two jets need to exhibit a certain angular separation. This is equivalent to establishing a minimum value for the variable $\Delta R_{jj} \equiv \sqrt{(\Delta\eta_{jj})^2 + (\Delta\phi_{jj})^2}$, where $\Delta\eta_{jj}$ and $\Delta\phi_{jj}$ are the separations

in pseudorapidity and azimuthal angle, respectively. The values chosen for these cuts, in agreement with [44] and [60], are:

$$\begin{aligned}
p_T^j &> 20 \text{ GeV}, \\
|\eta^j| &< 2, \\
\Delta R_{jj} &> 0.4, \\
\not{E}_T &> 20 \text{ GeV}.
\end{aligned}
\tag{4.6}$$

Once the Higgs bosons decay, and the cuts on the final state are implemented, the cross section diminishes in a factor of 3 to 5, approximately. Then, the cross section will be multiplied by ϵ^4 , where ϵ is the b -tagging efficiency factor, that will be assumed of an 80%, which agrees with [61] and [44]. After this cross section is computed, the number of events is obtained by multiplying the cross section by the accumulated luminosity. The ILC project expects a luminosity of 4 ab^{-1} at 500 GeV, and of 8 ab^{-1} at 1 TeV. On the other hand, the luminosity at 3 TeV at CLIC is proposed to be of 2.5 ab^{-1} [54]. Taking these values as references, we will display, in figure 4.6, contour plots for the number of events, in the same fashion as the ones shown before for the cross section.

Comparing these three plots to the corresponding ones for cross sections, some quantitative differences between both sets of plots appear (the contours are not equivalent). In other words, the plots which show number of events cannot be obtained by multiplying those which show cross sections by a constant number. This is due to the fact that the kinematical cuts imposed do not reduce the cross section in the same amount all over the parameter space. In fact, the closer to the center of the plot (the SM value), the bigger the effect of the cuts. This is reasonable: when a and b are far away from 1, the VBS mediated processes are more dominant. However, this effect is not too large, and the physical conclusions that can be extracted from both sets of plots are roughly the same.

As we have mentioned, the ranges for both parameters have been chosen to be the same in order to grasp a global view and to obtain conclusions on how the cross section (or, equivalently, the number of events) depends on the EChL parameters. However, current experimental results set strong constraints on a : most part of the parameter space we have showed is already experimentally excluded. On the contrary, no conclusive information is yet available concerning b . In fact, the current experimental bounds on this parameter are wider than those we have obtained by requiring unitarity. Thus, in order to be more sensitive to b , we will make a zoom on the allowed region for a . The results are displayed in figure 4.7.

At low energies, variations in b of up to 20% with respect to its SM value imply differences of just a handful of events. Although these experimental consequences would be extremely interesting, such a small number of events makes it impossible to obtain statistically solid conclusions. In order to do so, high energies would be required. In fact, in the TeV regime, hundreds or even thousand of events could be detected. In this scenario, it would be possible to set stronger constraints on b , or even on a , with a number of events large enough to yield statistically robust

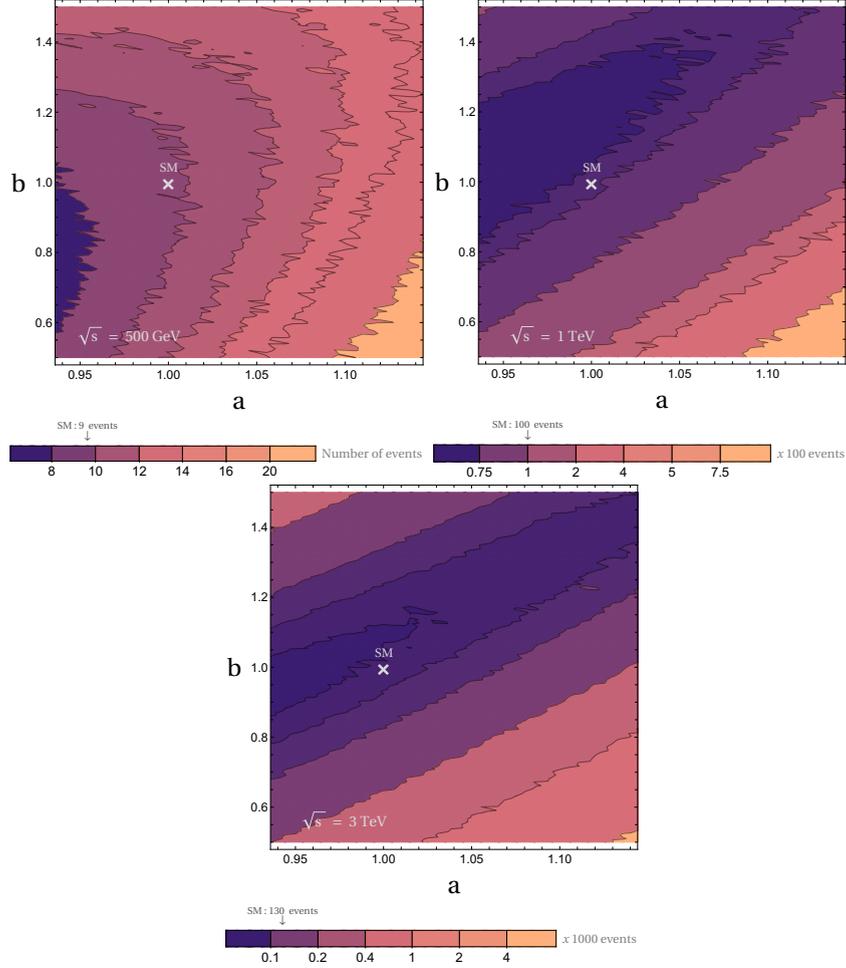


Figure 4.7: EChL predictions for contour lines of number of events of the full process, $e^+e^- \rightarrow HH\nu_e\bar{\nu}_e \rightarrow b\bar{b}b\bar{b}\nu_e\bar{\nu}_e$, in the (a, b) parameter space after the cuts shown in equation 4.6 are applied, at a center-of-mass energy of 500 GeV (upper panel), 1 TeV (middle panel) and 3 TeV (lower panel). The range of the parameter a is chosen so it coincides with the experimentally allowed region. The white cross represents the SM prediction ($a = b = 1$).

conclusions.

Of course, in order to determine if it is feasible to experimentally test the sensitivity to variations in a and b with respect to their SM values, it would be necessary to analyze the possible backgrounds. Nevertheless, this is beyond the intentios of this work and is left for future research.

5 Conclusions

The Standard Model of elementary particles and their fundamental interactions has been proven to be one of the most succesful theories in the History of Science, and

provides a consistent and exact description of the characteristic of the fundamental constituents of Nature and the way they interact. Nevertheless, there exist both experimental and theoretical issues that point to the incompleteness of the SM.

In particular, the Electroweak Symmetry Breaking Sector of the SM, in which the Higgs mechanism plays a key role, describes how the fundamental particles acquire a mass and how the Higgs boson becomes a physical state. So far, experimental results are in very good agreement with the theoretical understanding of this sector of the SM. However, there are certain reasons to believe that our description is not complete, such as the hierarchy problem or the fact that the Higgs boson is the only fundamental scalar in Nature.

Huge theoretical efforts have tried to unravel these misteries. Many high-energy models have been developed, studying new scenarios such as the Higgs boson being a composite particle, or the (pseudo) Nambu-Goldstone boson of a bigger symmetry which breaks down to the SM at energies way above our experimental reach. Although interesting, none of these proposals has been able to come up with solid solutions to the problems arising in the EWSBS of the SM.

The absence of a robust candidate for a complete UV theory has turned the interest of a part of the community to the employment of effective field theories as tools to search for Beyond the Standard Model effects at energies within our current experimental possibilities.

One of these theories is the Electroweak Chiral Lagrangian, inherited from the Chiral Lagrangian for low energy QCD, which describes the dynamics of electroweak NGBs below a certain UV scale. The lack of experimental evidences of a UV theory means that this scale must be around $4\pi v \sim 3$ TeV, which is the natural loop scale in this theory. The EChL introduces the NGBs in a non-linear, exponential representation, separately from the Higgs boson, which takes the form of a singlet and, thus, can be introduced, for instance, in a polynomical function. This effective theory includes certain parameters, which quantify deviations from the SM in a model independent way. This feature is the main advantage of the EChL: it does not need a UV theory to describe BSM interactions, making possible a direct contact with data. In fact, the hypothetical deviations from the SM, parametrized according to the EChL, can be later interpreted within many UV theories.

The EChL provides Feynman rules for the anomalous interaction vertices among Higgs, Z and W bosons. At first order in Chiral Perturbation Theory, the anomalous interactions are controlled by two parameters, a (involved in VVH couplings) and b (entering in $VVHH$ vertices), which are equal to 1 in the SM. Processes involving these vertices allow to search from deviations with respect to these values in experimental observables. In particular, Vector Boson Scattering (processes with two vector bosons in the initial state and two Higgs bosons in the final one) offer the best possibilites. So far, both theory and especially experiment have already set strong constraints on the possible range of values for a , while b is still practically unconstrained.

We have focused in the $W^+W^- \rightarrow HH$ subprocess, which involves four diagrams. We have found out that the behaviour of its cross section with the center-of-mass energy is very sensitive to variations of the parameters a and b . When any of them is different from 1, the cross section rapidly grows with the energy, whereas in the SM it basically stays constant when rising the energy at which the process takes place. This large enhancement of the cross section points out that unitarity might be a problem, as it is characteristic of UV incomplete theories, such as the EChL. In order to check this issue, we have performed a partial wave analysis, finding out that the s -wave partial amplitude exceeds 1 at a few TeV for certain values of the parameters. This leads to the conclusion that a and b cannot take arbitrary values, being constrained in order to guarantee unitarity.

After understanding how the $W^+W^- \rightarrow HH$ subprocess behaves, we have gone a step further, embedding it in a process taking place at an e^+e^- collider: $e^+e^- \rightarrow HH\nu_e\bar{\nu}_e$. This process includes several subprocesses, and not only the VBS ones we are interested in. In order to understand how relevant the VBS contribution is, we have compared Monte Carlo simulations to computations via the effective W approximation. The latter assumes that the vector bosons are produced as partons of the electrons and then scatter on-shell, therefore only considering VBS mediated processes. We have also compared the Monte Carlo simulations to those where muon neutrinos are produced in the final state: the difference will essentially be the VBS contribution. Both procedures have shown that, from 1 TeV onwards, VBS highly dominates, especially when either a or b depart from their SM values.

We have shown our predictions for cross section contour lines in the (a, b) parameter space, constraining a and b to ranges where unitarity is guaranteed. These results have shown that increasing or diminishing the parameters with respect to their SM values is not equivalent, and have also pointed that a plays a more relevant role (a fact that could be expected due to the presence of diagrams which scale as a^2). The behaviour of the contour lines is clearly sensitive to the energy of the process, which is consistent with the different energetic dependences of the contributing diagrams.

In order to end up providing predictions on experimental signatures, we have also performed the Monte Carlo simulations including the decays of the Higgs boson via their main channel, $H \rightarrow b\bar{b}$, and implementing cuts on the relevant kinematical variables of the final particles. In particular, we required a minimum in the missing energy associated to the neutrinos and in the transverse momentum of the jets produced by the hadronization of the b quarks. We also set cuts on the angular variables of the jets in order to guarantee a proper detection. Finally, we included the b -tagging efficiency, and multiplied the cross section by the luminosities expected at future e^+e^- machines, such as ILC or CLIC, to obtain the number of events that would be expected.

The results have been displayed in the same contour lines fashion, and also making a zoom in the region experimentally allowed for a . We found out that it is possible to set stronger constraints on b than the current ones, as the number of

events is reasonably sensitive to this parameter. However, it is necessary to reach high energies, in the TeV regime, to obtain statistically solid conclusions, as the number of events is really small at low energies. Furthermore, a study of the possible backgrounds would be necessary in order to determine if the future colliders are capable of testing realistic sensitivities to b . This analysis is beyond the scope of this work, and is expected to be performed in future work.

Summarizing, we have introduced the EChL, an effective theory that describes low-energy interactions between EW gauge and Higgs bosons, and shown how it allows to quantify deviations from the SM through a couple of parameters. We have analyzed how the $W^+W^- \rightarrow HH$ subprocess is sensitive to these deviations, and performed Monte Carlo simulations to search for experimental signatures that could reach interesting sensitivities to a and b or, otherwise, set constraints to the values of these parameters. Although a is already strongly constrained, we can conclude that future e^+e^- colliders could be sensitive to a and b via this kind of processes and, in particular, determine b for the first time. This may provide interesting information on the nature of the EWSBS of the SM.

Agradecimientos

En primer lugar quiero dar las gracias a mi tutora, María José Herrero, sin cuyo apoyo y esfuerzo no hubiera sido posible este trabajo. Además, no puedo olvidar que sin su apoyo en los primeros momentos, cuando este TFM no era más que una hipótesis, no hubiese podido obtener la Ayuda de Fomento a la Investigación de la cual he podido disfrutar durante este año. Muchas gracias, María José.

Quisiera extender mi gratitud a todos los que han sido mis profesores, de teoría y de problemas, durante el grado y el máster, sin los cuales no estaría hoy aquí. En mayor o menor medida, he aprendido de todos y cada uno de ellos, y, en mi humilde opinión, su labor merece más reconocimiento del que últimamente ha obtenido. Me gustaría hacer una mención especial a Enrique Álvarez, con quien empecé en esto de la Física Teórica, y al cual tengo un gran cariño.

He de dar las gracias al Instituto de Física Teórica por facilitarme un despacho y un lugar en el que trabajar. No podría haberme sentido mejor acogido, y espero poder pasar muchos más años trabajando aquí.

Ya en el terreno personal, no puedo empezar por alguien que no sean mis padres. Su apoyo y paciencia han sido infinitos desde aquellos (ya lejanos) comienzos de mi vida académica. Desde los trabajos de gimnasia hasta el problema de la barca, pasando por los dibujos a carboncillo, habéis sido mi bastón en los momentos más bajos y habéis compartido mi alegría en los más altos, que por suerte han sido unos cuantos. Todo este recorrido, que acaba con este trabajo, no podría entenderse sin vosotros. No podría estar más orgulloso de ser hijo vuestro.

También he de dar las gracias a los que fueron mis compañeros de la carrera, algunos de los cuales han pasado ya a ser compañeros de vida. Gracias por tantas risas, tantas palmeras de chocolate y por apoyarme cuando lo he necesitado. Habéis hecho de estos cuatro años una de las épocas más felices de mi vida.

Y hablando de compañeros, no puedo olvidarme de los que me han acompañado este año en el IFT: Claudia, Javi, Gallego y Rober. Pese a ser el último en llegar, me habéis hecho sentir uno más desde el primer día, y no he podido estar más cómodo compartiendo el día a día con vosotros. Gracias por las risas en el despacho, por vuestra paciencia cuando he necesitado vuestra ayuda y por las partidas de pocha (pese al injusto resultado). Habéis sido lo mejor de este año.

Y, por último en orden pero no en importancia, mi mayor agradecimiento es para Claudia. Necesitaría mucho más que un pequeño párrafo para mencionar todas las cosas que has hecho por mí este año. Gracias por animar a tu jefa a dirigir mi TFM, por hacerme un hueco en el despacho, por ayudarme con infinitos problemas informáticos, por enseñarme una (muy) pequeña parte de tu arte haciendo plots. Desde los ejercicios de minion en septiembre hasta los contour plots en julio, hubiera sido imposible dar cualquier paso en este trabajo sin ti; es tan tuyo como mío. Aún así, sería injusto si me quedase en agradecer tu apoyo con el TFM, y no recordase

los apuntes que me has dejado, los ejercicios en los que me has echado una mano, los ratos que has pasado enseñándome física y los consejos de cara al futuro. No hay cervezas suficientes para saldar mi deuda. Gracias.

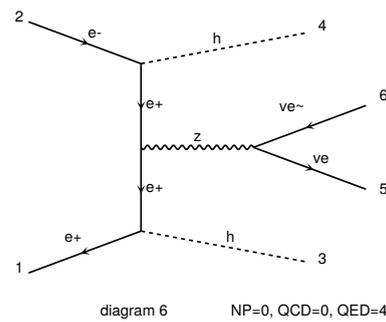
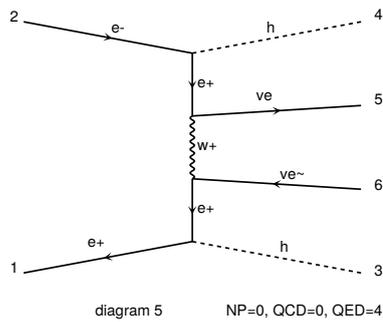
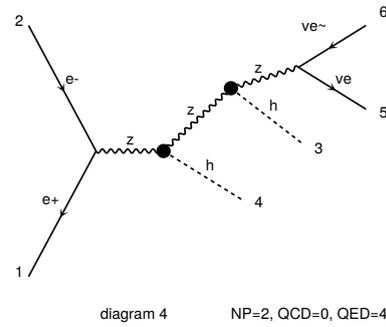
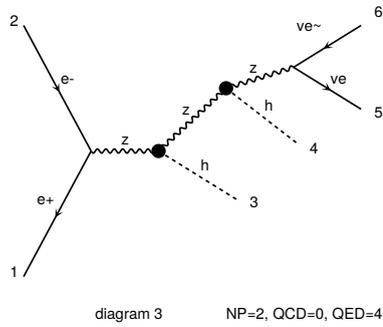
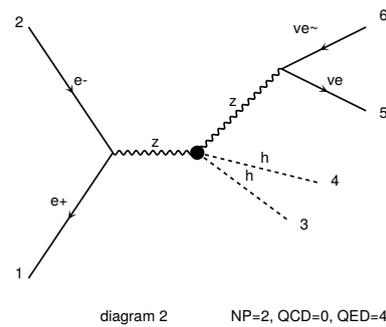
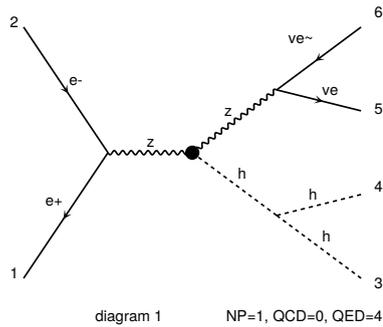
Appendices

A Diagrams contributing to the $e^+e^- \rightarrow HH\nu_e\bar{\nu}_e$ process

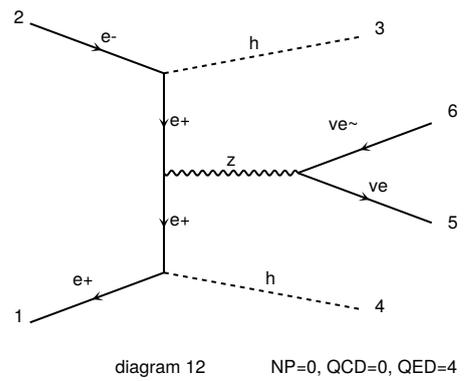
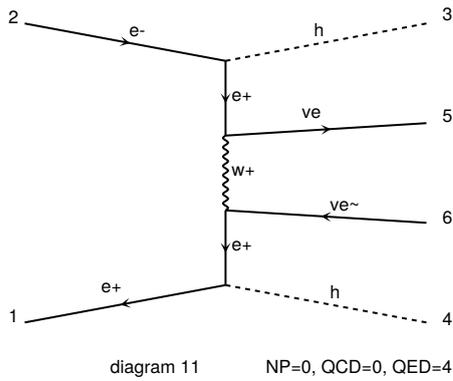
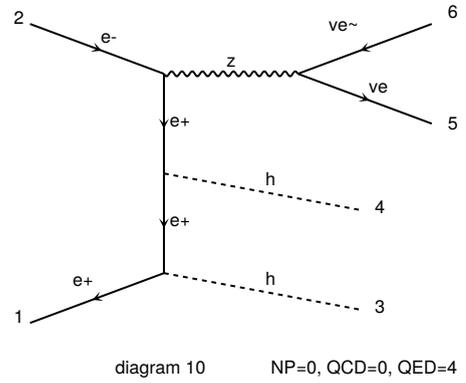
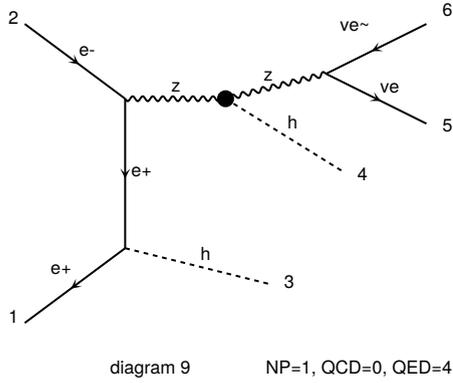
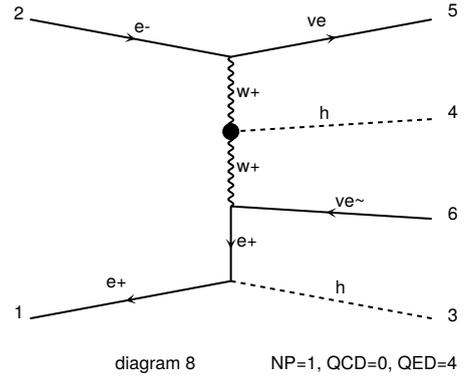
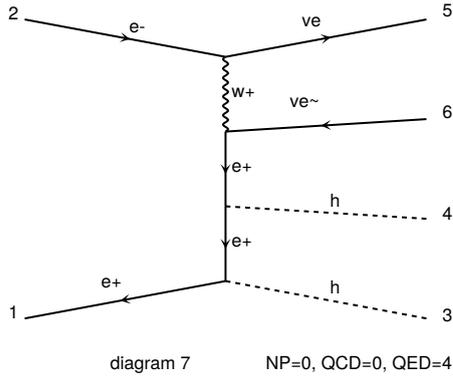
The following diagrams have been automatically generated by MadGraph:

$e^+e^- \rightarrow h h \nu_e \bar{\nu}_e$ NP=2

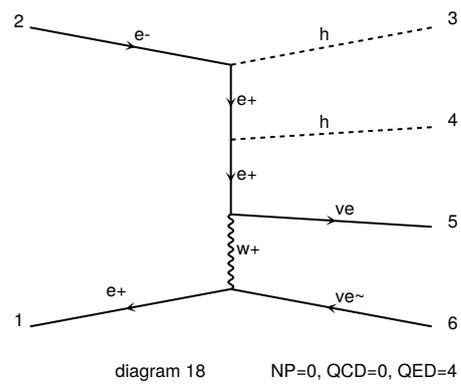
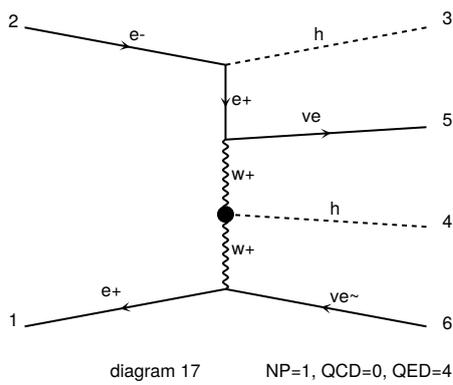
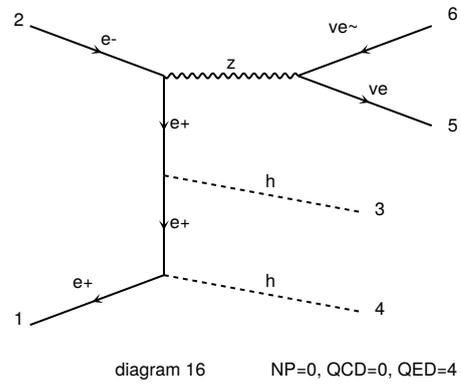
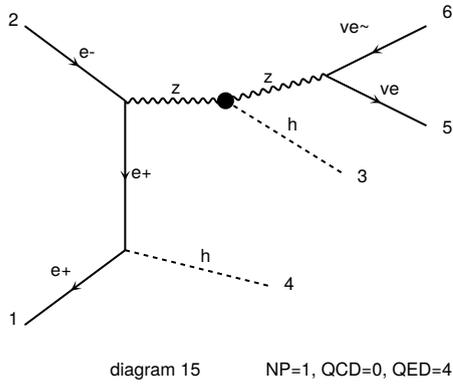
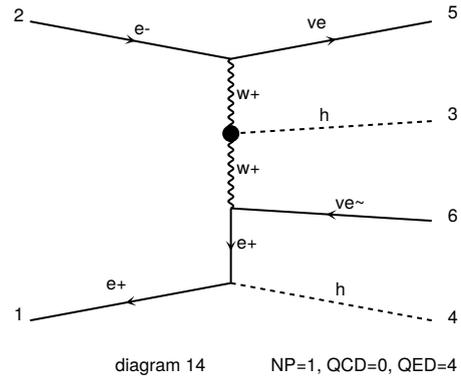
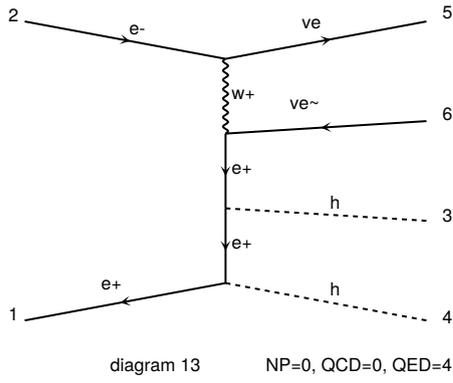
page 1/6



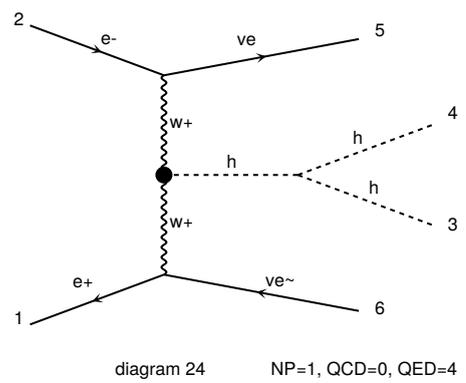
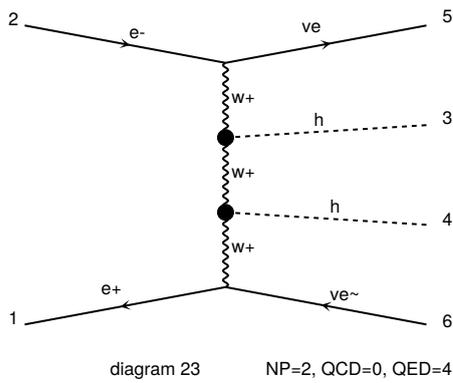
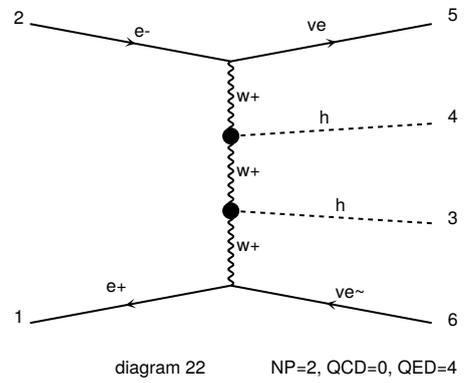
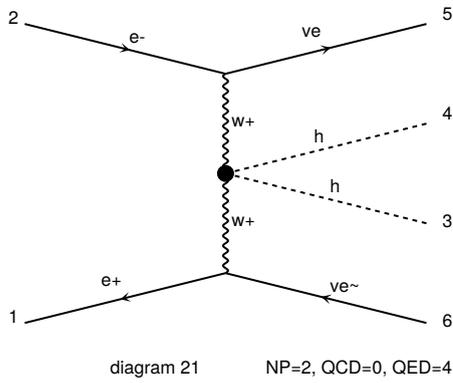
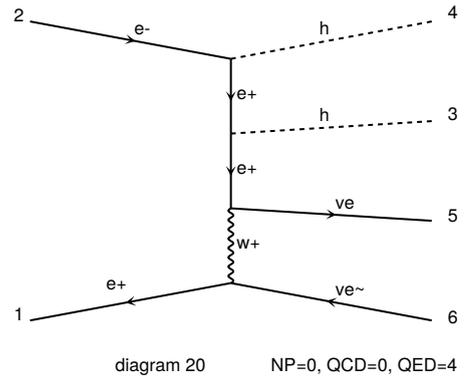
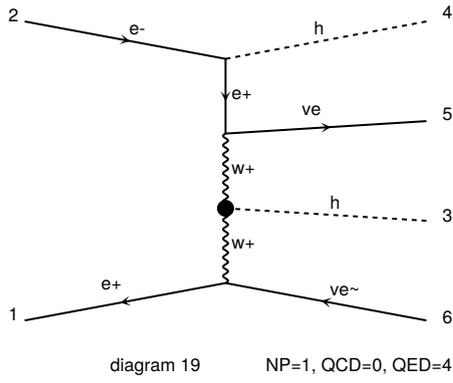
Diagrams made by MadGraph5_aMC@NLO



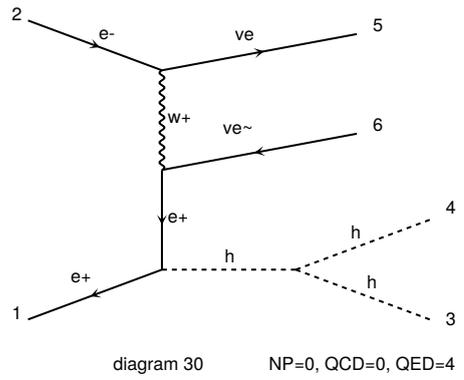
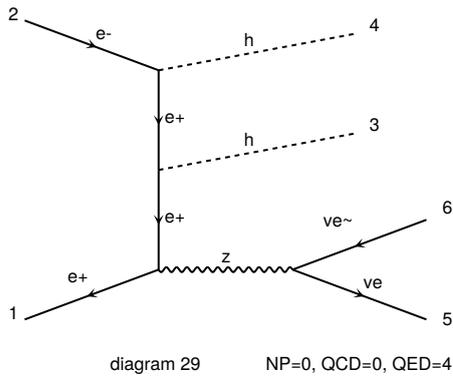
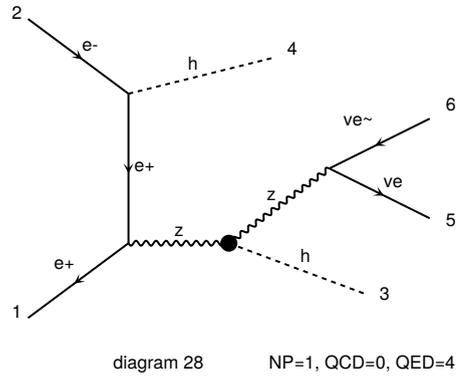
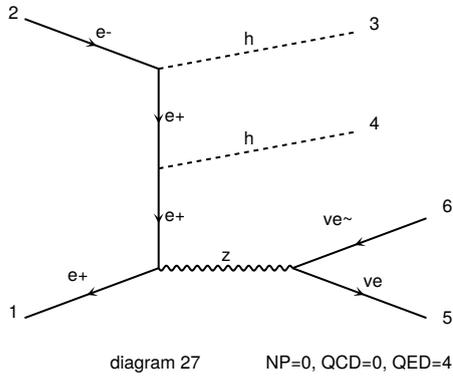
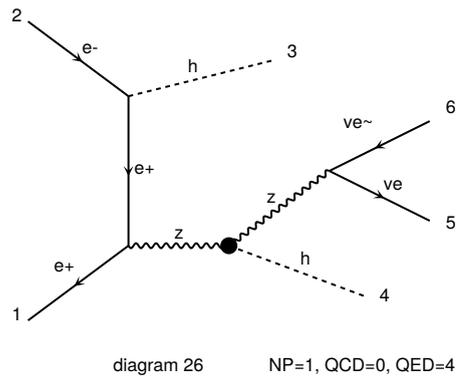
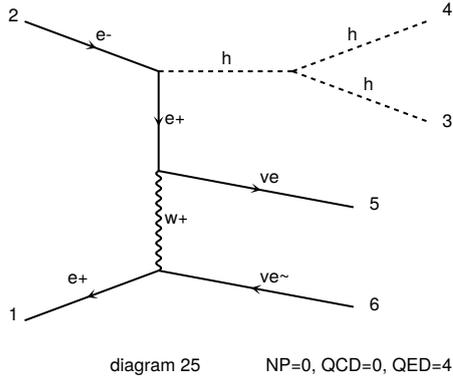
Diagrams made by MadGraph5_aMC@NLO



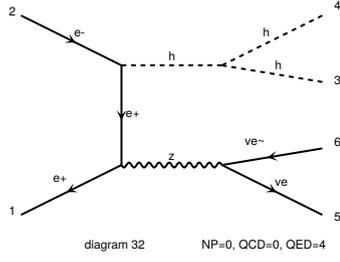
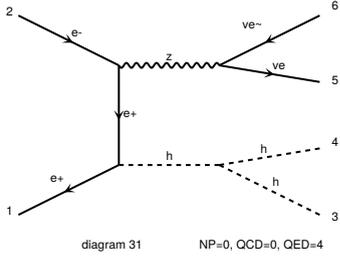
Diagrams made by MadGraph5_aMC@NLO



Diagrams made by MadGraph5_aMC@NLO



Diagrams made by MadGraph5_aMC@NLO



B Computations with the effective W approximation

The $W^+W^- \rightarrow HH$ subprocess will be characterized by an amplitude $F(\hat{s}, x)$, where \hat{s} is the square of the center-of-mass energy of the subprocess and $x \equiv \cos\theta$. The differential cross section will be

$$\frac{d\hat{\sigma}}{d\Omega} = \frac{|\vec{p}_{\text{out}}|}{|\vec{p}_{\text{in}}|} \frac{|\bar{F}|^2}{64\pi^2\hat{s}} \quad (\text{B.1})$$

The integration over the azimuthal angle is trivial, and the moduli of the incoming and outgoing three-momenta can be easily expressed as a function of \hat{s} :

$$\hat{\sigma}(\hat{s}) = \sqrt{\frac{\hat{s} - 4m_H^2}{\hat{s} - 4M_W^2}} \frac{1}{32\pi\hat{s}} \int_{-1}^1 dx |\bar{F}|^2(\hat{s}, x) \quad (\text{B.2})$$

where the averaged squared amplitude can be decomposed as

$$|\bar{F}|^2 = |\bar{F}|_{LL}^2 + |\bar{F}|_{TT}^2 + |\bar{F}|_{LT}^2 \quad (\text{B.3})$$

The squared center-of-mass energy of the whole $e^+e^- \rightarrow HH\bar{\nu}_e\nu_e$ process, s , is related to that of the subprocess through

$$\hat{s} = x_1x_2s \quad (\text{B.4})$$

where

$$x_1 = \frac{E_{W^+}}{E_{e^+}}, x_2 = \frac{E_{W^-}}{E_{e^-}} \quad (\text{B.5})$$

As electron and positron carry the same energy,

$$E_{e^+} = E_{e^-} \equiv E = \frac{\sqrt{s}}{2} \quad (\text{B.6})$$

The cross section of the whole process can be obtained by convoluting that of the subprocess with the distribution functions of the W bosons:

$$\sigma(s) = \int dx_2 \int dx_1 f(x_1)f(x_2)\hat{\sigma}(x_1x_2s) \quad (\text{B.7})$$

Some kinematical cuts must be applied to the variables x_1 and x_2 . The energy of the subprocess must be large enough to produce two Higgs bosons. This means

$$\hat{s} \geq 4m_H^2 \Rightarrow x_1x_2s \geq 4m_H^2 \Rightarrow x_1 \geq \frac{4m_H^2}{x_2s} \quad (\text{B.8})$$

Besides, each of the W bosons needs to have an energy of at least its mass. Picking, for instance, the W^- ,

$$E_{W^-} \geq M_W \Rightarrow \frac{x_2\sqrt{s}}{2} \geq M_W \Rightarrow x_2 \geq \frac{2M_W}{\sqrt{s}} \quad (\text{B.9})$$

Taking these considerations into account, the total cross section can be expressed as:

$$\sigma(s) = \int_A^1 dx_2 \int_{B/x_2}^1 dx_1 f(x_1) f(x_2) \hat{\sigma}(x_1 x_2 s) \quad (\text{B.10})$$

with $A \equiv 2M_W/\sqrt{s}$ and $B \equiv 4m_H^2/s$. However, in order to perform these integrals numerically, the integration variables must be independent. In order to achieve so, some changes of variable need to be performed. Defining $\tau \equiv x_1 x_2$ and $\eta \equiv \frac{1}{2} \log \left(\frac{x_1}{x_2} \right)$ yields $x_1 = \sqrt{\tau} e^\eta$ and $x_2 = \sqrt{\tau} e^{-\eta}$. As $\tau = \frac{\hat{s}}{s}$, it spans in the range $\tau \in [\frac{4m_H^2}{s}, 1]$. The other variable will be in the range $\eta \in [\log \sqrt{\tau}, -\log \sqrt{\tau}]$. The Jacobian of this change of variables is 1, so

$$\begin{aligned} \sigma(s) &= \int_{4m_H^2}^1 d\tau \int_{\log \sqrt{\tau}}^{-\log \sqrt{\tau}} d\eta \hat{\sigma}(\hat{s}) = \int_{4m_H^2}^1 d\tau \int_{\log \sqrt{\tau}}^{-\log \sqrt{\tau}} d\eta \int_{-1}^1 dx f(\sqrt{\tau} e^\eta) f(\sqrt{\tau} e^{-\eta}) \times \\ &\quad \times \sqrt{\frac{\tau s - 4m_H^2}{\tau s - 4M_W^2}} \frac{1}{32\pi\tau s} |\bar{F}|^2(\tau s, x) \end{aligned} \quad (\text{B.11})$$

However, these integration variables still depend on each other, and a numerical integration needs them to be independent. Thus, a further change of variables will be worked out:

$$\omega_1 \equiv \frac{\log \left(\frac{\tau s}{4m_H^2} \right)}{\log \left(\frac{s}{4m_H^2} \right)} \quad (\text{B.12})$$

$$\omega_2 \equiv \frac{1}{2} \left(1 - \frac{\eta}{\tau} \right) \quad (\text{B.13})$$

$$\omega_3 \equiv \frac{1}{2} (1 + x) \quad (\text{B.14})$$

These new variables are all contained in the range $[0, 1]$. Now the Jacobian is not trivial:

$$J(\omega_1, \omega_2, \omega_3) = 8\tau(\omega_1) \log \frac{1}{\sqrt{\tau(\omega_1)}} \log \frac{s}{4m_H^2} \quad (\text{B.15})$$

with

$$\tau(\omega_1) = \frac{4m_H^2}{s} \exp \left(2\omega_1 \log \frac{s}{4m_H^2} \right) \quad (\text{B.16})$$

Thus,

$$\begin{aligned} \sigma(s) &= \int_0^1 \omega_1 \int_0^1 \omega_2 \int_0^1 \omega_3 J(\omega_1, \omega_2, \omega_3) f(x_1(\tau(\omega_1), \eta(\omega_1, \omega_2))) f(x_2(\tau(\omega_1), \eta(\omega_1, \omega_2))) \times \\ &\quad \times \sqrt{\frac{\tau(\omega_1)s - 4m_H^2}{\tau(\omega_1)s - 4M_W^2}} \frac{1}{32\pi\tau(\omega_1)s} |\bar{F}|^2(\tau(\omega_1)s, x) \end{aligned} \quad (\text{B.17})$$

where

$$\eta(\omega_1, \omega_2) = (2\omega_2 - 1) \log \frac{1}{\sqrt{\tau(\omega_1)}} \quad (\text{B.18})$$

Equation B.7 is actually a bit more complicated. As the distribution functions depend on the polarization of the vector bosons, it is necessary to split the squared amplitude (according to equation B.3), weighting each piece with the corresponding distribution functions.

$$\begin{aligned} \sigma(s) = & \int_0^1 \omega_1 \int_0^1 \omega_2 \int_0^1 \omega_3 J(\omega_1, \omega_2, \omega_3) \sqrt{\frac{\tau(\omega_1)s - 4m_H^2}{\tau(\omega_1)s - 4M_W^2}} \frac{1}{32\pi\tau(\omega_1)s} \times \\ & \times \sum_{i,j} f_i(x_1(\tau(\omega_1), \eta(\omega_1, \omega_2))) f_j(x_2(\tau(\omega_1), \eta(\omega_1, \omega_2))) |\bar{F}_{i,j}|^2(\tau(\omega_1)s, x) \end{aligned} \quad (\text{B.19})$$

where the indices i and j run over the longitudinal and transverse polarizations of the gauge bosons. This expression can be numerically integrated. This integration will be performed employing two different sets of distribution functions (both can be found in [56]): the ones obtained employing the Leading Log Approximation (LLA), which assumes $E \gg M_W$, and the improved ones, which keep terms of order M_W/E .

Equations B.20 and B.21 show the ‘‘PDFs’’, within the LLA, for W bosons which carry a fraction x of the energy of the electron, E , and exhibit a transverse and longitudinal polarization, respectively.

$$f_T(x) = \frac{g^2}{32\pi^2 x} [x^2 + 2(1-x)] \log\left(\frac{4E^2}{M_W^2}\right) \quad (\text{B.20})$$

$$f_L(x) = \frac{g^2}{16\pi^2} \frac{1-x}{x} \quad (\text{B.21})$$

Equations B.22 and B.23 show the improved distribution functions, which keep terms of order M_W/E .

$$\begin{aligned} f_T(x) = & \frac{g^2}{32\pi^2 x} \left[\frac{-x^2}{1 + M_W^2/(4E^2(1-x))} + \frac{2x^2(1-x)}{M_W^2/E^2 - x^2} + \right. \\ & \left. \left\{ x^2 + \frac{x^4(1-x)}{(M_W^2/E^2 - x^2)^2} \times \left(2 + \frac{M_W^2}{E^2(1-x)} \right) - \frac{x^2}{(M_W^2/E^2 - x^2)^2} \frac{M_W^4}{2E^4} \right\} \right. \\ & \left. \times \log\left(1 + \frac{4E^2(1-x)}{M_W^2}\right) + x^4 \left(\frac{2-x}{M_W^2/E^2 - x^2} \right)^2 \log \frac{x}{2-x} \right] \eta \quad (\text{B.22}) \end{aligned}$$

with $\eta \equiv \left(1 - \frac{M_W^2}{x^2 E^2}\right)^{1/2}$.

$$\begin{aligned} f_L(x) = & \frac{g^2}{4\pi^2} \frac{1-x}{x} \frac{\eta}{(1+\eta)^2} \\ & \times \left\{ \frac{1-x - M_W^2/(8E^2)}{1-x + M_W^2/(4E^2)} - \frac{M_W^2}{4E^2} \frac{1+2(1-x)^2}{1-x + M_W^2/(4E^2)} \frac{1}{M_W^2/E^2 - x^2} \right. \\ & \left. - \frac{M_W^2}{4E^2} \frac{x^2}{2(1-x)(x^2 - M_W^2/E^2)^2} \left[(2-x)^2 \log \frac{x}{2-x} - \left(\left(x - \frac{M_W^2}{E^2 x}\right)^2 \right) \right] \right\} \end{aligned}$$

$$\begin{aligned}
& -(2(1-x) + x^2) \log \left(1 + \frac{4E^2(1-x)}{M_W^2} \right) \Big] \\
& - \frac{M_W^2}{8E^2} \frac{x}{\sqrt{x^2 - M_W^2/E^2}} \left[\frac{2}{x^2 - M_W^2/E^2} + \frac{1}{1-x} \right] \\
& \times \left[\log \frac{2-x-\sqrt{x^2 - M_W^2/E^2}}{2-x+\sqrt{x^2 - M_W^2/E^2}} - \log \frac{x-\sqrt{x^2 - M_W^2/E^2}}{x+\sqrt{x^2 - M_W^2/E^2}} \right] \Big\} \quad (\text{B.23})
\end{aligned}$$

References

- [1] S. L. Glashow, Nucl. Phys. **22** (1961) 579. doi:10.1016/0029-5582(61)90469-2
- [2] S. Weinberg, Phys. Rev. Lett. **19** (1967) 1264. doi:10.1103/PhysRevLett.19.1264
- [3] A. Salam, Edited by: Svartholm N. Almquist and Wiksells, Stockholm 367 (1968).
- [4] P. W. Anderson, Phys. Rev. **130** (1963) 439. doi:10.1103/PhysRev.130.439
- [5] P. W. Higgs, Phys. Lett. **12** (1964) 132. doi:10.1016/0031-9163(64)91136-9
- [6] P. W. Higgs, Phys. Rev. Lett. **13** (1964) 508. doi:10.1103/PhysRevLett.13.508
- [7] F. Englert and R. Brout, Phys. Rev. Lett. **13** (1964) 321. doi:10.1103/PhysRevLett.13.321
- [8] P. W. Higgs, Phys. Rev. **145** (1966) 1156. doi:10.1103/PhysRev.145.1156
- [9] T. W. B. Kibble, Phys. Rev. **155** (1967) 1554. doi:10.1103/PhysRev.155.1554
- [10] J. Goldstone, A. Salam and S. Weinberg, Phys. Rev. **127** (1962) 965. doi:10.1103/PhysRev.127.965
- [11] G. Arnison *et al.* [UA1 Collaboration], Phys. Lett. B **122** (1983) 103 [Phys. Lett. **122B** (1983) 103]. doi:10.1016/0370-2693(83)91177-2
- [12] M. Banner *et al.* [UA2 Collaboration], Phys. Lett. B **122** (1983) 476 [Phys. Lett. **122B** (1983) 476]. doi:10.1016/0370-2693(83)91605-2
- [13] G. Arnison *et al.* [UA1 Collaboration], Phys. Lett. B **126** (1983) 398 [Phys. Lett. **126B** (1983) 398]. doi:10.1016/0370-2693(83)90188-0
- [14] P. Bagnaia *et al.* [UA2 Collaboration], Phys. Lett. B **129** (1983) 130 [Phys. Lett. **129B** (1983) 130]. doi:10.1016/0370-2693(83)90744-X
- [15] G. Aad *et al.* [ATLAS Collaboration], Phys. Lett. B **716** (2012) 1 doi:10.1016/j.physletb.2012.08.020 [arXiv:1207.7214 [hep-ex]].
- [16] S. Chatrchyan *et al.* [CMS Collaboration], Phys. Lett. B **716** (2012) 30 doi:10.1016/j.physletb.2012.08.021 [arXiv:1207.7235 [hep-ex]].
- [17] A. Dobado, A. Gomez-Nicola, A. L. Maroto, and J. R. Pelaez, *Effective lagrangians for the standard model* (1997).
- [18] J. F. Donoghue, E. Golowich, and B. R. Holstein, *Dynamics of the standard model*, Vol. 2 (1992) pp. 1–540.
- [19] F. L. Wilson, Am. J. Phys. **36** (1968) no.12, 1150. doi:10.1119/1.1974382
- [20] S. Weinberg, Physica A **96** (1979) no.1-2, 327. doi:10.1016/0378-4371(79)90223-1

- [21] A. C. Longhitano, Phys. Rev. D **22** (1980) 1166. doi:10.1103/PhysRevD.22.1166
- [22] A. C. Longhitano, Nucl. Phys. B **188** (1981) 118. doi:10.1016/0550-3213(81)90109-7
- [23] T. Appelquist and C. W. Bernard, Phys. Rev. D **22** (1980) 200. doi:10.1103/PhysRevD.22.200
- [24] K. Agashe, R. Contino and A. Pomarol, Nucl. Phys. B **719** (2005) 165 doi:10.1016/j.nuclphysb.2005.04.035 [hep-ph/0412089].
- [25] R. Contino, L. Da Rold and A. Pomarol, Phys. Rev. D **75** (2007) 055014 doi:10.1103/PhysRevD.75.055014 [hep-ph/0612048].
- [26] R. Contino, doi:10.1142/97898143271830005 arXiv:1005.4269 [hep-ph].
- [27] M. Carena, L. Da Rold and E. Pontón, JHEP **1406** (2014) 159 doi:10.1007/JHEP06(2014)159 [arXiv:1402.2987 [hep-ph]].
- [28] A. Dobado and M. J. Herrero, Phys. Lett. B **228** (1989) 495. doi:10.1016/0370-2693(89)90981-7
- [29] A. Dobado and M. J. Herrero, Phys. Lett. B **233** (1989) 505. doi:10.1016/0370-2693(89)91349-X
- [30] A. Dobado, M. J. Herrero, J. R. Pelaez, E. Ruiz Morales and M. T. Urdiales, Phys. Lett. B **352** (1995) 400 doi:10.1016/0370-2693(95)00431-J [hep-ph/9502309].
- [31] A. Dobado, M. J. Herrero, J. R. Pelaez and E. Ruiz Morales, Phys. Rev. D **62** (2000) 055011 doi:10.1103/PhysRevD.62.055011 [hep-ph/9912224].
- [32] M. J. Herrero and E. Ruiz Morales, Nucl. Phys. B **418** (1994) 431 doi:10.1016/0550-3213(94)90525-8 [hep-ph/9308276].
- [33] M. J. Herrero and E. Ruiz Morales, Nucl. Phys. B **437** (1995) 319 doi:10.1016/0550-3213(94)00589-7 [hep-ph/9411207].
- [34] R. L. Delgado, A. Dobado, M. J. Herrero and J. J. Sanz-Cillero, JHEP **1407** (2014) 149 doi:10.1007/JHEP07(2014)149 [arXiv:1404.2866 [hep-ph]].
- [35] J. de Blas, O. Eberhardt and C. Krause, JHEP **1807** (2018) 048 doi:10.1007/JHEP07(2018)048 [arXiv:1803.00939 [hep-ph]].
- [36] J. Gasser and H. Leutwyler, Annals Phys. **158** (1984) 142. doi:10.1016/0003-4916(84)90242-2
- [37] J. Gasser and H. Leutwyler, Nucl. Phys. B **250** (1985) 465. doi:10.1016/0550-3213(85)90492-4
- [38] The ATLAS collaboration [ATLAS Collaboration], ATLAS-CONF-2019-030.

- [39] R. L. Delgado, A. Dobado and F. J. Llanes-Estrada, Phys. Rev. Lett. **114** (2015) no.22, 221803 doi:10.1103/PhysRevLett.114.221803 [arXiv:1408.1193 [hep-ph]].
- [40] M. Tanabashi *et al.* [Particle Data Group], Phys. Rev. D **98** (2018) no.3, 030001. doi:10.1103/PhysRevD.98.030001
- [41] M. Baak *et al.*, Eur. Phys. J. C **72** (2012) 2205 doi:10.1140/epjc/s10052-012-2205-9 [arXiv:1209.2716 [hep-ph]].
- [42] M. Ciuchini, E. Franco, S. Mishima and L. Silvestrini, EPJ Web Conf. **60** (2013) 08004. doi:10.1051/epjconf/20136008004
- [43] A. V. Manohar and V. Mateu, Phys. Rev. D **77** (2008) 094019 doi:10.1103/PhysRevD.77.094019 [arXiv:0801.3222 [hep-ph]].
- [44] R. Contino, C. Grojean, D. Pappadopulo, R. Rattazzi and A. Thamm, JHEP **1402** (2014) 006 doi:10.1007/JHEP02(2014)006 [arXiv:1309.7038 [hep-ph]].
- [45] R. L. Delgado, A. Dobado, D. Espriu, C. Garcia-Garcia, M. J. Herrero, X. Marcano and J. J. Sanz-Cillero, JHEP **1711** (2017) 098 doi:10.1007/JHEP11(2017)098 [arXiv:1707.04580 [hep-ph]].
- [46] G. Buchalla, O. Cata, A. Celis, M. Knecht and C. Krause, Nucl. Phys. B **928** (2018) 93 doi:10.1016/j.nuclphysb.2018.01.009 [arXiv:1710.06412 [hep-ph]].
- [47] D. Espriu, F. Mescia and B. Yenko, Phys. Rev. D **88** (2013) 055002 doi:10.1103/PhysRevD.88.055002 [arXiv:1307.2400 [hep-ph]].
- [48] I. Brivio and M. Trott, Phys. Rept. **793** (2019) 1 doi:10.1016/j.physrep.2018.11.002 [arXiv:1706.08945 [hep-ph]].
- [49] E. Arganda, C. Garcia-Garcia and M. J. Herrero, Nucl. Phys. B (2019) 114687 [Nucl. Phys. B **945** (2019) 114687] doi:10.1016/j.nuclphysb.2019.114687 [arXiv:1807.09736 [hep-ph]].
- [50] T. Hahn, Comput. Phys. Commun. **140** (2001) 418 doi:10.1016/S0010-4655(01)00290-9 [hep-ph/0012260].
- [51] T. Hahn and M. Perez-Victoria, Comput. Phys. Commun. **118** (1999) 153 doi:10.1016/S0010-4655(98)00173-8 [hep-ph/9807565].
- [52] A. Alloul, N. D. Christensen, C. Degrande, C. Duhr and B. Fuks, Comput. Phys. Commun. **185** (2014) 2250 doi:10.1016/j.cpc.2014.04.012 [arXiv:1310.1921 [hep-ph]].
- [53] T. Behnke *et al.*, arXiv:1306.6327 [physics.acc-ph].
- [54] M. Aicheler *et al.* [CLIC accelerator Collaboration], doi:10.23731/CYRM-2018-004 arXiv:1903.08655 [physics.acc-ph].
- [55] J. Alwall *et al.*, JHEP **1407** (2014) 079 doi:10.1007/JHEP07(2014)079 [arXiv:1405.0301 [hep-ph]].

- [56] S. Dawson, Nucl. Phys. B **249** (1985) 42. doi:10.1016/0550-3213(85)90038-0
- [57] G. P. Lepage, J. Comput. Phys. **27** (1978) 192. doi:10.1016/0021-9991(78)90004-9
- [58] A. Alboteanu, W. Kilian and J. Reuter, JHEP **0811** (2008) 010 doi:10.1088/1126-6708/2008/11/010 [arXiv:0806.4145 [hep-ph]].
- [59] P. W. Johnson, F. I. Olness and W. K. Tung, Phys. Rev. D **36** (1987) 291. doi:10.1103/PhysRevD.36.291
- [60] H. Abramowicz *et al.*, Eur. Phys. J. C **77** (2017) no.7, 475 doi:10.1140/epjc/s10052-017-4968-5 [arXiv:1608.07538 [hep-ex]].
- [61] F. Bishara, R. Contino and J. Rojo, Eur. Phys. J. C **77** (2017) no.7, 481 doi:10.1140/epjc/s10052-017-5037-9 [arXiv:1611.03860 [hep-ph]].